Revision 1

Word Count: 6679

MAGNESIO-LUCCHESIITE, $CaMg_3Al_6(Si_6O_{18})(BO_3)_3(OH)_3O$, A NEW SPECIES OF THE TOURMALINE SUPERGROUP

EMILY D. SCRIBNER[1,2], JAN CEMPÍREK[3,*], LEE A. GROAT[2], R. JAMES EVANS[2], CRISTIAN BIAGIONI[4], FERDINANDO BOSI[5,*], ANDREA DINI[6], ULF HÅLENIUS[7], PAOLO ORLANDI[4], MARCO PASERO[4]

[1]*Environmental Engineering and Earth Sciences, Clemson University, 445 Brackett Hall, 321 Calhoun Drive, Clemson, South Carolina 29634, USA*

[2]*Department of Earth, Ocean and Atmospheric Sciences, University of British Columbia, Vancouver, British Columbia V6T 1Z4, Canada*

[3]*Department of Geological Sciences, Faculty of Science, Masaryk University, Brno, CZ-65937, Czech Republic*

[4]*Dipartimento di Scienze della Terra, Università di Pisa, Via Santa Maria 53, I-56126 Pisa, Italy*

[5]*Dipartimento di Scienze della Terra, Sapienza Università di Roma, Piazzale Aldo Moro 5, I-00185, Rome, Italy*

[6]*Institute of Geosciences and Georisorse-CNR, Via Moruzzi 1, 56124 Pisa, Italy*

[7]*Department of Geosciences, Swedish Museum of Natural History, P.O. Box 50 007, 104 05 Stockholm, Sweden*

[*] *E-mail address:* jcemp@sci.muni.cz; ferdinando.bosi@uniroma1.it

This is the peer-reviewed, final accepted version for American Mineralogist, published by the Mineralogical Society of America.
The published version is subject to change. Cite as Authors (Year) Title. American Mineralogist, in press.
DOI: https://doi.org/10.2138/am-2021-7496. http://www.minsocam.org/

Abstract

Magnesio-lucchesiite, ideally $CaMg_3Al_6(Si_6O_{18})(BO_3)_3(OH)_3O$, is a new mineral species of the tourmaline supergroup. The holotype material was discovered within a lamprophyre dike that cross-cuts tourmaline-rich metapelites within the exocontact of the O'Grady Batholith, Northwest Territories (Canada). Two additional samples were found at San Piero in Campo, Elba Island, Tuscany (Italy) in hydrothermal veins embedded in meta-serpentinites within the contact aureole of the Monte Capanne intrusion. The studied crystals of magnesio-lucchesiite are black in hand sample with vitreous luster, conchoidal fracture, an estimated hardness of 7–8, and a calculated density of 3.168 (Canada) and 3.175 g.cm^{-3} (Italy). In plane-polarized light, magnesio-lucchesiite is pleochroic (O = dark brown, E = colorless) and uniaxial (–); its refractive index values are n_ω = 1.668(3) and n_ε = 1.644(3) (Canada), and n_ω = 1.665(5) and n_ε = 1.645(5) (Italy). Magnesio-lucchesiite is trigonal, space group *R*3*m*, Z = 3, with a = 15.9910(3) Å, c = 7.2224(2) Å, V = 1599.42(7) Å^3 (Canada) and with a = 15.9270(10) Å, c = 7.1270(5) Å, V = 1565.7(2) Å^3 (Italy, sample #1). The crystal structure of magnesio-lucchesiite was refined to R_1 = 3.06% and 1.96% using 2953 (Canadian sample) and 1225 (Italian sample) reflections with $F_o > 4\sigma(F_o)$. The Canadian (holotype) sample has the ordered empirical formula $^{X}(Ca_{0.60}Na_{0.39}K_{0.01})_{\Sigma1.00}$ $^{Y}(Mg_{2.02}Fe^{2+}_{0.62}Fe^{3+}_{0.09}Ti_{0.25}V_{0.01}Cr_{0.01})_{\Sigma3.00}$ $^{Z}(Al_{5.31}Fe^{3+}_{0.69})_{\Sigma6.00}$ $[^{T}(Si_{5.98}Al_{0.02})_{\Sigma6.00}O_{18}]$ $(BO_3)_3$ $^{V}[(OH)_{2.59}O_{0.41}]_{\Sigma3.00}$ $^{W}(O_{0.78}F_{0.22})_{\Sigma1.00}$. The Italian cotype material shows a wider chemical variability, with two different samples from the same locality having ordered chemical formulae: $^{X}(Ca_{0.88}Na_{0.12})_{\Sigma1.00}$ $^{Y}(Mg_{1.45}Fe^{2+}_{0.40}Al_{0.79}Fe^{3+}_{0.36})_{\Sigma3.00}$ $^{Z}Al_6$ $[^{T}(Si_{5.05}Al_{0.95})_{\Sigma6.00}O_{18}]$ $(BO_3)_3$ $^{V}[(OH)_{2.90}O_{0.10}]_{\Sigma3.00}$ $^{W}(O_{0.98}F_{0.02})_{\Sigma1.00}$ (sample #1) and $^{X}(Ca_{0.71}Na_{0.21}\square_{0.08})_{\Sigma1.00}$ $^{Y}(Mg_{2.49}Fe^{2+}_{0.41}Ti_{0.10})_{\Sigma3.00}$ $^{Z}(Al_{5.44}Fe^{3+}_{0.46}Mg_{0.09}V_{0.01})_{\Sigma6.00}$

This is the peer-reviewed, final accepted version for American Mineralogist, published by the Mineralogical Society of America.
The published version is subject to change. Cite as Authors (Year) Title. American Mineralogist, in press.
DOI: https://doi.org/10.2138/am-2021-7496. http://www.minsocam.org/

$[^{T}(Si_{5.87}Al_{0.13})_{\Sigma 6.00}O_{18}]\,(BO_3)_3\,{}^{V}(OH)_3\,{}^{W}[O_{0.61}(OH)_{0.39}]_{\Sigma 1.00}$ (sample #2). Magnesio-lucchesiite is an oxy-species belonging to the calcic group of the tourmaline supergroup. It is related to lucchesiite by the homovalent substitution ${}^{Y}Fe \leftrightarrow {}^{Y}Mg$, and to feruvite by the homovalent and heterovalent substitutions ${}^{Y}Fe \leftrightarrow {}^{Y}Mg$ and ${}^{Z}Al^{3+} + {}^{W}O^{2-} \leftrightarrow {}^{Z}Mg^{2+} + {}^{W}(OH)^{1-}$. The new mineral was approved by the International Mineralogical Association Commission on New Minerals, Nomenclature and Classification (IMA 2019-025). Occurrences of magnesio-lucchesiite show that its presence is not restricted to replacement of mafic minerals only; it may form also in metacarbonate rocks by fluctuations of F and Al during crystallization of common uvitic tourmaline. High miscibility with other tourmaline endmembers indicates large petrogenetic potential of magnesio-lucchesiite in Mg,Al-rich calcsilicate rocks, as well as contact-metamorphic, and metasomatic rocks.

Keywords: magnesio-lucchesiite, new mineral species, lamprophyre dike, O'Grady Batholith, San Piero in Campo, Elba Island.

Introduction

Tourmaline-supergroup minerals are complex borosilicates that occur in a wide variety of host environments; it is characteristic for granitic and metamorphic rocks (from low-grade to ultra-high pressures), detrital phase in sedimentary rocks, as well as accessory phase of multiple hydrothermal deposits. Due to its refractory behavior, it is the dominant host for B in silicic rocks of the Earth crust (e.g. Dutrow and Henry, 2011). Tourmaline has been extensively studied because of its ability to incorporate several major as well as trace elements into its crystal structure, making it an ideal monitor of its local environment (van Hinsberg et al. 2011).

The general chemical formula of tourmaline-supergroup minerals is $XY_3Z_6(T_6O_{18})(BO_3)_3V_3W$, where X = Na^+, K^+, Ca^{2+}, □ (= vacancy); Y = Al^{3+}, Fe^{3+}, Cr^{3+}, V^{3+}, Mg^{2+}, Fe^{2+}, Mn^{2+}, Li^+, Ti^{4+}, □; Z = Al^{3+}, Fe^{3+}, Cr^{3+}, V^{3+}, Mg^{2+}, Fe^{2+}; T = Si^{4+}, Al^{3+}, B^{3+}; B = B^{3+}; V = $(OH)^-$, O^{2-}; W = $(OH)^-$, F^-, O^{2-} (Henry et al. 2011). The letters X, Y, Z and B represent groups of constituents accommodated at the $^{[9]}X$, $^{[6]}Y$, $^{[6]}Z$, $^{[4]}T$ and $^{[3]}B$ crystallographic sites (identified with *italicized* letters); the letters V and W represent groups of anions accommodated at the $^{[3]}$O(3) and $^{[3]}$O(1) crystallographic sites, respectively. The H atoms, when present in the V or W anion groups, occupy the H(3) and H(1) sites, which are bonded to O(3) and O(1), respectively. Note that, unlike amphibole or spinel, the structural and the chemical formulae of tourmaline coincide: each crystallographic site in the structural formula matches a (non-italicized) letter in the chemical formula (Bosi et al. 2019a). Tourmaline species are partitioned into groups and subgroups based on the dominant occupancy of the *X* site and various coupled substitutions, respectively (Henry et al. 2011). There are currently 36 species of tourmaline approved by the IMA-CNMNC, of which 15 are oxy-species, mostly described in the years following the publication of the tourmaline nomenclature (Henry et al. 2011; Bosi 2018).

This paper presents chemical, structural, and optical data of a new species of the tourmaline supergroup, first identified along the margin of a lamprophyre dike that cross-cuts tourmaline-rich metapelites within the exocontact of the O'Grady Batholith, Northwest Territories, Canada. In the frame of the hierarchical classification of tourmalines (Henry et al. 2011), this tourmaline belongs to the calcic-subgroup 3 of the calcic group. The first member of this subgroup was defined as lucchesiite, ideally $CaFe_3^{2+}Al_6(Si_6O_{18})(BO_3)_3(OH)_3O$, by Bosi et al. (2017a). In accordance with the nomenclature of Henry et al. (2011), this new species is named magnesio-lucchesiite due to the dominance of Mg over Fe at the *Y* site:

92 $CaMg_3Al_6(Si_6O_{18})(BO_3)_3(OH)_3O$. The new species and its name have been approved by the
93 IMA-CNMNC (proposal number IMA2019-025). After the proposal of the mineral, an additional
94 finding of magnesio-lucchesiite was identified from the contact aureole of the Monte Capanne
95 intrusion, Elba Island, Italy. This second finding provided more abundant material allowing the
96 collection of further data that improved the description of this new species. Holotype material is
97 deposited in the Canadian Museum of Nature in Ottawa, Canada, under catalogue number
98 CMNMC 87266; cotype material from Italy is deposited in the Museo di Storia Naturale
99 (Università di Pisa), under catalogue number 15921, and in the Swedish Museum of Natural
100 History (Stockholm), under the number NRM#20190127.
101
102 **Occurrence**
103 Magnesio-lucchesiite was first identified along the margin of a lamprophyre dike, near
104 the O'Grady Batholith in the Nááts'ihch'oh National Park Reserve, Northwest Territories,
105 Canada (62°46'8.33"N, 128°56'9.07"W). Specifically, magnesio-lucchesiite occurs as small
106 zones near the rims of larger, chemically zoned tourmaline crystals (Fig. 1). The lamprophyre
107 dikes have not been dated, but they are likely younger than the megacrystic hornblende phase of
108 the O'Grady Batholith (K–Ar hornblende age of 95 ± 1 Ma; Hunt and Roddick 1987) and older
109 than the associated aplite and pegmatite dikes, as well as tourmaline-bearing quartz veins based
110 on cross-cutting relationships (Scribner et al. 2018).
111 The O'Grady Batholith is hosted by variably hornfelsed shale, silty shale, and minor
112 chert of the Mount Christie Formation. The Batholith is part of the larger, mid-Cretaceous
113 Selwyn Plutonic Suite. It is a composite intrusion that is mostly composed of a megacrystic
114 hornblende granite that grades, via a foliated transitional phase, to an equigranular, hornblende-

115 biotite granodiorite on the margins (Gordey and Anderson 1993). The megacrystic hornblende
116 granite is the intrusive phase present at the locality of magnesio-lucchesiite. This granite contains
117 rare, highly altered tourmaline.

118 The lamprophyre dikes trend north–south, range from 2–6 m in width, and are hosted in
119 metapelitic rocks that have been frequently metasomatized to tourmalinite (rock with > 30%
120 tourmaline; Slack and Trumbull 2011). The mineralogy of these host rocks can vary, with some
121 samples being tourmalinites and others being less tourmaline-rich with more plagioclase, biotite,
122 amphibole, and rare apatite and zircon. The lamprophyre dikes are composed of amphiboles
123 (ranging from actinolite to magnesio-hornblende), plagioclase ($An_{92}Or_6Ab_2$–$Ab_{58}An_{41}Or_1$), K-
124 feldspar ($Or_{97}An_3Ab_0$), and quartz with minor titanite, and rare diopside, apatite, pyrite, allanite-
125 (Ce), and zircon (Scribner et al. 2018). Tourmaline, including magnesio-lucchesiite, crystallized
126 when B-bearing fluids derived from aplite and pegmatite dikes associated with the O'Grady
127 Batholith reacted with the lamprophyre dikes (Scribner et al. 2018). Tourmaline occurs as
128 subhedral grains up to 5 mm across at the margins of the lamprophyre dikes and as massive
129 aggregates with common inclusions of other minerals in an altered zone near the margins. This
130 altered zone extends inwards from the margins of the lamprophyre dikes can reach several
131 millimeters in thickness. In addition to tourmaline it also contains remnants of the primary
132 actinolite to magnesiohornblende, and secondary clinochlore, titanite, and quartz, with minor
133 clinopyroxene and apatite. From the two tourmaline textural types recognized by Scribner et al.
134 (2018), magnesio-lucchesiite occurs as small dark brown zones on rims of Tur I (originally
135 described as Fe-rich uvite) near the margin of the dike (Fig. 1). Besides very rare magnesio-
136 lucchesiite, the tourmaline aggregates contain common (Ca,^{W}O)-rich dravite with patches of
137 uvite, feruvite, and fluor-uvite.

The second occurrence of magnesio-lucchesiite was identified some tens of meters south of San Piero in Campo (Elba Island, Livorno, Tuscany, Italy – 42°44'54''N, 10°12'40''E). The first specimen was collected in the 1980s by one of authors (PO) (sample #1 – Fig. 2a), whereas a recent sampling in June 2019 resulted in the collection of additional specimens (sample #2). In both cases, magnesio-lucchesiite occurs in veins filling fractures within meta-serpentinite occurring in the contact aureole of the Monte Capanne monzogranite intrusion. This is the largest pluton exposed in the Tuscan Magmatic Province (e.g., Dini et al. 2002; Farina et al. 2012) and its age of emplacement is 7 Ma at a depth of ca. 5–6 km (Barboni et al. 2015 and references therein). The contact aureole records peak metamorphic conditions of temperatures up to 650 °C and pressures of 0.1–0.2 GPa (Dini et al. 2002). San Piero in Campo is well-known for the occurrence of pegmatitic dikes representing the type locality of five tourmaline species, i.e, elbaite (Vernadsky 1913), tsilaisite (Bosi et al. 2012), fluor-tsilaisite (Bosi et al. 2015), celleriite (Bosi et al. 2020a) and uvite (Bosi et al. 2020b). In addition, schorl, rossmanite, fluor-elbaite, and foitite were identified in the pegmatitic dikes. Whereas the tourmalines in this type of occurrence have been studied since the 19th century, no data have yet been published on tourmaline from the thermometamorphic rocks of the contact aureole. At San Piero in Campo, the eastern edge of the Monte Capanne monzogranite pluton is mantled by foliated remnants of the contact aureole represented by meta-ophiolites and pelitic hornfels (Ligurian Units). The lithium-cesium-tantalum (LCT) pegmatite dikes intruded the outermost margin of the pluton, locally cutting through the contact aureole (e.g. Tonarini et al. 1998). The interaction between the B-rich fluids, that escaped from the pegmatite dikes, and meta-serpentinites produced a network of hydrothermal veins filled by Ca-enriched tourmalines, including magnesio-

lucchesiite. Strictly related to these hydrothermal veins is the formation of the recently approved new species uvite (Bosi et al. 2020b).

In sample #1, magnesio-lucchesiite is associated with tabular pseudo-hexagonal green crystals of chlorite group minerals and pinkish flakes of mica; in sample #2, tourmaline is associated with chlorite, euhedral yellow crystals of titanite, and grains of partially oxidized pyrite.

Physical and Optical Properties

Magnesio-lucchesiite from the Canadian type locality forms an anhedral crystal in a medium-grained black tourmaline aggregate at the contact of a lamprophyre dike (see Scribner et al. 2018). It is black in hand sample, with vitreous luster, brittle with conchoidal fracture, has an estimated hardness of 7-8, and a calculated density of 3.168 $g.cm^{-3}$ (on the basis of the empirical formula and unit-cell volume refined from single-crystal X-ray diffraction data). In plane-polarized light, magnesio-lucchesiite is pleochroic (O = dark brown, E = colorless) and uniaxial (–); its refractive index values are n_{ω} = 1.668(3) and n_{ε} = 1.644(3).

Magnesio-lucchesiite from the cotype locality at San Piero in Campo occurs as euhedral prismatic crystals, up to 3 mm in length, brownish to bluish in color. Calculated density, on the basis of the empirical formula of sample #1 and its unit-cell parameters (see below) is 3.175 g cm^{-3}. In plane-polarized light, it is strongly pleochroic (O = greenish-blue; E = yellowish-brown. O >> E). It is uniaxial (–) and its refractive index values, measured with white light, are n_{ω} = 1.665(5) and n_{ε} = 1.645(5).

The compatibility index (calculated according to the Gladstone-Dale relationship; Mandarino 1979, 1981) of holotype and cotype material (sample #1) is 0.034 (excellent) and 0.024 (excellent), respectively.

Analytical Methods and Results

Electron microprobe analysis (EMPA)

Major and trace element composition of magnesio-lucchesiite from the Canadian type locality was measured using a Cameca SX-100 electron probe microanalyzer operating in wavelength-dispersion mode at Masaryk University in the Czech Republic. The following analytical conditions were used: acceleration voltage 15 kV, beam current 10 nA, spot diameter 5 μm. The following standards, X-ray *K*α lines and analyzer crystals were used: albite (Na; TAP), sanidine (Si, Al; TAP), sanidine (K; PET), pyrope (Mg; TAP), titanite (Ti; LPET), chromite (Cr; LPET), vanadinite (Cl; LPET), fluorapatite (P; LPET), wollastonite (Ca; PET), almandine (Fe; LLIF), spessartine (Mn; LLIF), $ScVO_4$ (V; LLIF), gahnite (Zn; LLIF), topaz (F; PC1). Data were processed using the X-Phi matrix correction of Merlet (1994). Results of the analyses of the single crystal on which X-ray diffraction measurements were made are summarized in Table 1.

Major and trace element composition of cotype magnesio-lucchesiite from San Piero in Campo was measured using a Cameca SX50 instrument (Istituto di Geologia Ambientale e Geoingegneria, CNR, Rome), operating at 15 kV, sample current of 15 nA, and a beam diameter of 10 μm. The following standards, X-ray *K*α lines and analyzer crystals were used: jadeite (Na; TAP), periclase (Mg; TAP), orthoclase (K; PET), rutile (Ti; PET), wollastonite (Si, Ca; PET), metallic Zn and Mn (Zn, Mn; LIF), vanadinite (V; PET), fluorphlogopite (F; TAP), metallic Cr (Cr; PET), corundum (Al; TAP), magnetite (Fe; LIF). The 'PAP' routine was applied (Pouchou

and Pichoir 1991). The analysis of sample #1 was performed on the same crystal used for single-crystal X-ray diffraction study. Back-scattered electron image shows a slight zonation, likely related to the Al and Fe contents of the studied sample (Fig. 2b). Results are given in Table 2.

The $Fe^{3+}/\Sigma Fe_{tot}$ ratio for the holotype material could not be measured directly with Mössbauer spectroscopy due to the small size of the tourmaline crystals; it was therefore calculated from bond-valence site occupancy optimization of the formula derived from the electron microprobe analyses and measured structure of magnesio-lucchesiite. Values for Al, Mg, Fe^{3+}, and Ti^{4+} were allowed as variables for disorder between the *Y* and *Z* sites. Differences for bond valence versus cation charge, and structure refinement versus optimized occupancy electron numbers at each *Y* and *Z* site were minimized in Microsoft Excel using Solver routine. Bond-valence parameters for O^{2-} and F^{-} bonds were employed (Brown 2002). As an additional control, differences between the observed average bond lengths versus ideal bond lengths calculated using the procedure of Bosi and Lucchesi (2007) based on optimized ionic radii in tourmaline were checked. The observed versus calculated average bond length differences for *Y* and *Z* sites are very low (0.000 and 0.004 Å, respectively); when minimization of differences was included as a parameter to the optimization, it led to identical values. The optimization resulted in 0.785 atoms per formula unit (apfu) Fe^{3+} in total, mostly located at the *Y* site. For the cotype samples from San Piero in Campo, the amount of FeO and Fe_2O_3 were determined by Mössbauer spectroscopy (see below). The optimization procedure described above resulted in Fe^{3+}/Fe_{tot} ratio very similar to that found by Mössbauer spectroscopy (0.46 vs. 0.47) when applied to the cotype sample with unconstrained Fe^{3+}/Fe_{tot}.

In the studied samples, B was assumed to be stoichiometric (3.000 B pfu), in agreement with the results of single-crystal refinements (see below); in nature, high $^{[4]}B$ is present in highly

fractionated Al-rich tourmalines (e.g. Ertl et al. 2018), and hence unlikely in magnesio-lucchesiite. The amount of H or OH was calculated in agreement with structural results and in order to achieve the electrostatic neutrality, under the assumption of (Y+Z+T) = 15.000 apfu and 31 anions.

Mössbauer spectroscopy

The ^{57}Fe Mössbauer spectra of magnesio-lucchesiite from San Piero in Campo (samples #1 and 2) were collected at room temperature in transmission mode using a ^{57}Co (in Rh matrix) point source of gamma radiation with nominal activity of 0.40 GBq at the Natural History Museum of Stockholm (Sweden), over the velocity range ± 4 mm/s and calibrated against α-Fe foil. Data were collected in 1024 channels with a constant acceleration system equipped with a proportional gas-filled counter on absorbers consisting of less than 1 mg mineral powder between mylar windows during 580 and 71 hours, respectively. The spectra were fitted using the program MossA (Prescher et al. 2012) and are shown in Fig. 3. Table 3 summarizes the results of the experiments and the spectra fitting. Three doublets were assigned to Fe^{2+}, and one doublet to Fe^{3+}. The $Fe^{3+}/\Sigma Fe_{tot}$ is 0.47 and 0.53 for samples #1 and 2, respectively. Hyperfine parameters agree with the occurrence of Fe^{2+} at *Y* and Fe^{3+} mainly located at *Z* (Andreozzi et al. 2008).

Infrared spectroscopy

Polarized single-crystal infrared spectra of magnesio-lucchesiite from San Piero in Campo (Fig. 4) were recorded with a Bruker Vertex 70 microscope spectrometer (Swedish Museum of Natural History, Stockholm), equipped with a halogen lamp source, a CaF_2 beam-splitter, a holographic ZnSe polarizer, and an InSb detector. The crystals were oriented by

morphology and optical microscopy and were doubly polished parallel to the **a**-**c** plane. The thickness of the single-crystal absorber was 39 and 35 μm for samples #1 and 2, respectively. Spectra were collected parallel ($E||E$) and perpendicular ($E||O$) to the **c**-axis, over the wavenumber range 2000-13000 cm^{-1}, with a resolution of 4 cm^{-1} during 64 cycles. In the spectrum of sample #1, bands above 3650 cm^{-1}, associated with $(OH)^-$ groups at the O(1) site (e.g., Gonzalez-Carreño et al. 1988; Skogby et al. 2012; Bosi et al. 2015), are very weak and consistent with the low content of (OH) at the O(1) site reported in the empirical formula (see below). In sample #2 the greater magnitude of the bands above 3650 cm^{-1} are consistent with minor occurrence of (OH) at O(1) as reported in the empirical formula (see below).

Optical absorption spectroscopy

Polarized optical absorption spectra were acquired on magnesio-lucchesiite from San Piero in Campo on the same polished grains used for the collection of infrared spectra. An AVASPEC-ULS2048X16 spectrometer (Swedish Museum of Natural History, Stockholm) attached via a 400 μm UV fiber cable to a Zeiss Axiotron UV-microscope was used. A 75 W Xenon arc lamp was used as light source and Zeiss Ultrafluar 10× lenses were used as objective and condenser. The size of the circular measure aperture was 55 μm in diameter. A UV-quality Glan-Thompson prism with a working range from 40000 to 3704 cm^{-1} was used as polarizer. The recorded spectra (Fig. 5) show broad and intense absorption bands at 14250 and 8790 cm^{-1}. These bands are strongly polarized in $E \perp$ **c** ($E||O$). In agreement with previous optical studies of tourmaline (e.g., Mattson and Rossman 1987) these two absorption bands are assigned to Fe^{3+}-enhanced spin-allowed *d*-*d* transitions in six-coordinated Fe^{2+}. In the spectra of crystal #2 from San Piero in Campo a broad, intense and strongly $E||O$-polarized band at 22000 cm^{-1} is recorded

(Fig. 5b). This band is due to Fe^{2+}-Ti^{4+} intervalence charge transfer processes (e.g., Smith 1978; Taran et al. 1993). The absence of this band in the spectra of crystal #1 (Fig. 5a) is explained by a very low Ti-content below the analytical detection limit of the electron microprobe (see Table 2).

Crystallography

A single crystal was extracted from the zone of holotype magnesio-lucchesiite (Canadian sample) within Tur I in a thin section using a microscope-mounted microdrill. Single-crystal X-ray diffraction measurements were made at the Centre for Higher Order Structure Elucidation (C-HORSE) at the University of British Columbia using a Bruker X8 APEX II diffractometer with graphite monochromated Mo*K*α radiation. The refined unit-cell parameters are a = 15.9910(3) Å; c = 7.2224(2) Å; V = 1599.42(7) Å^3, space group $R3m$ (#160), Z = 3. The crystal structure of holotype magnesio-lucchesiite was refined based on the oxy-schorl structure model (Bačík et al. 2013). The CrysAlis (Oxford Diffraction Ltd.) and SHELXTL (PC Version; Sheldrick 2008) program packages were used for data reduction and structure refinement, respectively, using neutral scattering factors and anomalous dispersion corrections. Starting coordinates were taken from structural model of lucchesiite (Bosi et al. 2017a). The two most common atoms (with sufficient difference in number of electrons) present at the respective site were used for refinement of occupancies of the *X* (Ca, Na), *Y* (Mg, Fe), and *Z* (Al, Fe) sites; the occupancy of 1 for ^{T}Si and ^{B}B was assumed since the electron density at the *T* and *B* site did not significantly deviate from full occupancy. The position of the H(3) hydrogen atom was located on the residual electron density map; the H(1) hydrogen atom bonded to O(1) (0.25 *apfu* H, see EMPA data) could not be located. The structure was refined in $R3m$ space group and converged

296 to a final R_1 index of 3.06 % for 2953 reflections with $F_o > 4\sigma(F_o)$ and 95 refined parameters.
297 The crystal structure is isotypic with those of other members of tourmaline supergroup minerals.

298 With regard to sample #1 (Italian sample), one fragment was extracted from a polished
299 section prepared on a crystal from sample #1 (Fig. 2b), previously investigated through SEM in
300 order to ascertain its chemical homogeneity. Intensity data were collected at the Dipartimento di
301 Scienze della Terra, Università di Pisa, using a Bruker AXS Smart Breeze diffractometer
302 equipped with an air-cooled Photon II detector and graphite-monochromatized Mo*K*α radiation.
303 Refined unit-cell parameters are a = 15.9270(10) Å, c = 7.1270(5) Å, V = 1565.7(2) Å^3, space
304 group $R3m$ (#160), Z = 3. Structure refinement was done using the SHELXL-2013 program
305 (Sheldrick 2015). Starting coordinates were taken from Bosi et al. (2017a). Variable parameters
306 were scale factor, extinction coefficient, atom coordinates, site-scattering values (for *X*, *Y* and *Z*)
307 and atomic-displacement factors. Regarding the atomic model refinement, the *X* site was
308 modeled using the Na and Ca scattering factors. The occupancy of the *Y* site was obtained
309 considering the presence of Mg and Fe, while the *Z* site was modelled considering the presence
310 of Al versus Fe. The *T*, *B* and anion sites were modeled, respectively, with Si, B and O scattering
311 factors and with a fixed occupancy of 1, because refinement with unconstrained occupancies
312 showed no significant deviations from this value. There were no correlations greater than 0.7
313 between the parameters at the end of the refinement. Table 4 lists crystal data, data-collection
314 information and refinement details; Table 5 gives the fractional atom coordinates, site occupancy
315 factors and equivalent isotropic-displacement parameters; Table 6 shows refined and calculated
316 site scattering values, and Table 7 selected bond lengths. Bond-valence calculations, using the
317 formula and bond-valence parameters from Brown and Altermatt (1985), are reported in Table 8.
318 A CIF[1] is deposited.

X-ray powder diffraction data were not collected due to the small size of the magnesio-lucchesiite domain from the type locality. Instead, PLATON (Spek 2003) routines hkl2Powder and SimPowderP (represented by functions "Powder Iobs" and "Powder Icalc" in the PLATON for Windows Taskbar v.1.19) were used to generate powder reflections from the observed single crystal intensities data (I_{obs} in Table 9) and from the structural parameters (I_{calc} in Table 9). The powder data were generated in the range of $2\Theta = 0–90°$ for Cu$K\alpha$ wavelength; their values are provided in Table 9. Unit-cell parameters for the powder are therefore the same as for single-crystal data.

Discussion

Empirical formulae for magnesio-lucchesiite

The empirical formula for the holotype material, calculated based on fully occupied *Y*, *Z*, and *T* sites [as recommended by Henry et al. (2011) for tourmaline with none or low Li and $^{[4]}$B] with cation disorder over *Y* and *Z* is: $^{X}(Ca_{0.60}Na_{0.39}K_{0.01})_{\Sigma 1.00}$ $^{Y}(Mg_{1.27}Fe^{2+}_{0.62}Fe^{3+}_{0.61}Ti_{0.25}Al_{0.23}V_{0.01}Cr_{0.01})_{\Sigma 3.00}$ $^{Z}(Al_{5.08}Fe^{3+}_{0.17}Mg_{0.75})_{\Sigma 6.00}$ $[^{T}(Si_{5.98}Al_{0.02})_{\Sigma 6.00}O_{18}]$ $(BO_3)_3$ $^{V}[(OH)_{2.33}O_{0.67}]_{\Sigma 3.00}$ $^{W}[O_{0.52}(OH)_{0.26}F_{0.22}]_{\Sigma 1.00}$. This was calculated from structure refinement and bond-valence optimization. All F atoms are located at the W position of the general formula as F cannot occupy the V position (Robert et al. 1997; Henry et al. 2011). Disorder of (OH) between the V and W positions was estimated using the empirical equation $^{W}(OH) = \{2 – [1.01*BVS(O1)] – 0.21 – F\}$ of Bosi (2013).

The empirical ordered formula, with R^{3+}-cations ordered in the Z position and (OH) ordered in the V position of the general formula, required for the purpose of nomenclature as recommended by Henry et al. (2011) is:

This is the peer-reviewed, final accepted version for American Mineralogist, published by the Mineralogical Society of America.
The published version is subject to change. Cite as Authors (Year) Title. American Mineralogist, in press.
DOI: https://doi.org/10.2138/am-2021-7496. http://www.minsocam.org/

342 $^{X}(Ca_{0.60}Na_{0.39}K_{0.01})_{\Sigma 1.00}$ $^{Y}(Mg_{2.02}Fe^{2+}_{0.62}Fe^{3+}_{0.09}Ti_{0.25}V_{0.01}Cr_{0.01})_{\Sigma 3.00}$ $^{Z}(Al_{5.31}Fe^{3+}_{0.69})_{\Sigma 6.00}$

343 $[^{T}(Si_{5.98}Al_{0.02})_{\Sigma 6.00}O_{18}](BO_3)_3\,^{V}[(OH)_{2.59}O_{0.41}]_{\Sigma 3.00}\,^{W}(O_{0.78}F_{0.22})_{\Sigma 1.00}$.

344 In accordance with the dominant-valency rule (Bosi et al. 2019a,b), this formula leads to the end-
345 member composition $CaMg_3Al_6(Si_6O_{18})(BO_3)_3(OH)_3O$: in detail, Ca-dominant at the X position
346 of the tourmaline general formula and divalent anion dominates at W with O^{2-}; the Y, Z and T
347 positions are dominated by $^{Y}R^{2+}$-cations (with predominance of Mg), $^{Z}R^{3+}$-cations (with
348 predominance of Al) and $^{T}R^{4+}$-cations (with predominance of Si). The ideal magnesio-lucchesiite
349 formula requires (in wt.%) CaO 5.75, MgO 12.41, Al_2O_3 31.38, SiO_2 36.98, B_2O_3 10.71, H_2O
350 2.77, total 100.

351 The crystal-chemical characterization of samples #1 and #2 from San Piero in Campo
352 (Italy) shows significant chemical variability in comparison to the Canadian sample. The most
353 representative empirical formula of sample #1 can be derived from the combination of electron
354 microprobe, single-crystal X-ray diffraction, Mössbauer and infrared spectroscopy data using the
355 optimization procedure of Bosi et al. (2017b):

356 $^{X}(Ca_{0.88}Na_{0.12})_{\Sigma 1.00}$ $^{Y}(Al_{1.43}Fe^{3+}_{0.19}Mg_{0.98}Fe^{2+}_{0.40})_{\Sigma 3.00}$ $^{Z}(Al_{5.36}Mg_{0.47}Fe^{3+}_{0.17})_{\Sigma 6.00}$

357 $[^{T}(Si_{5.05}Al_{0.95})_{\Sigma 6.00}O_{18}](BO_3)_3\,^{V}[(OH)_{2.68}O_{0.32})]_{\Sigma 3.00}\,^{W}[O_{0.76}(OH)_{0.22}F_{0.02}]_{\Sigma 1.00}$.

358 Note that the disorder of (OH) between the V and W positions was estimated using the above
359 empirical equation of Bosi (2013). This formula, however, does not lead to an end-member
360 formula, mainly due to Al and Mg disordering over the octahedrally coordinated sites. The
361 dominance of R^{3+}-cations in the Y position leads to the charge imbalance formula
362 $[CaAl_3Al_6(Si_6O_{18})(BO_3)_3(OH)_3O]^{\Sigma 3+}$. As recommended by Henry et al. (2011), the empirical
363 ordered formula is therefore used for nomenclature purposes:

This is the peer-reviewed, final accepted version for American Mineralogist, published by the Mineralogical Society of America.
The published version is subject to change. Cite as Authors (Year) Title. American Mineralogist, in press.
DOI: https://doi.org/10.2138/am-2021-7496. http://www.minsocam.org/

364 $^{X}(Ca_{0.88}Na_{0.12})_{\Sigma 1.00}$ $^{Y}(Al_{0.79}Fe^{3+}{}_{0.36}Mg_{1.45}Fe^{2+}{}_{0.40})_{\Sigma 3.00}$ $^{Z}Al_{6}$ $[^{T}(Si_{5.05}Al_{0.95})_{\Sigma 6.00}O_{18}]$

365 $^{V}[(OH)_{2.90}O_{0.10}]_{\Sigma 3.00}$ $^{W}(O_{0.98}F_{0.02})_{\Sigma 1.00}$.

366 In accordance with the dominance-valency rule (Bosi et al. 2019a,b), this formula leads to the

367 end-member composition $CaMg_3Al_6(Si_6O_{18})(BO_3)_3(OH)_3O$.

368 Sample #2 was characterized by chemical, Mössbauer and infrared spectroscopic data. In

369 accordance with Henry et al. (2011), its empirical ordered formula is

370 $^{X}(Ca_{0.71}Na_{0.21}\square_{0.08})_{\Sigma 1.00}$ $^{Y}(Mg_{2.49}Fe^{2+}{}_{0.41}Ti_{0.10})_{\Sigma 3.00}$ $^{Z}(Al_{5.44}Fe^{3+}{}_{0.46}V_{0.01}Mg_{0.09})_{\Sigma 6.00}$

371 $[^{T}(Si_{5.87}Al_{0.13})_{\Sigma 6.00}O_{18}]$ $(BO_3)_3$ $^{V}(OH)_3$ $^{W}[O_{0.61}(OH)_{0.39}]_{\Sigma 1.00}$

372 which also leads to the end-member composition $CaMg_3Al_6(Si_6O_{18})(BO_3)_3(OH)_3O$.

373

374 **Chemical variability of magnesio-lucchesiite and relations with other species**

375 Magnesio-lucchesiite is a new member of the calcic subgroup 3 of the tourmaline

376 supergroup (Henry et al. 2011). It is the Mg-analogue of lucchesiite, ideally

377 $^{X}Ca^{Y}Fe^{2+}{}_3{}^{Z}Al_6{}^{T}Si_6O_{18}(BO_3)_3{}^{V}(OH)_3{}^{W}O$ (Bosi et al. 2017a), which is related by the homovalent

378 substitution $^{Y}Fe^{2+} \leftrightarrow {}^{Y}Mg^{2+}$. It is also related to feruvite,

379 $^{X}Ca^{Y}Fe^{2+}{}_3{}^{Z}(MgAl_5)^{T}Si_6O_{18}(BO_3)_3{}^{V}(OH)_3{}^{W}(OH)$ (Grice and Robinson 1989), through the

380 homovalent and heterovalent substitutions $^{Y}Fe^{2+} \leftrightarrow {}^{Y}Mg^{2+}$ and $^{Z}Al^{3+} + {}^{W}O^{2-} \leftrightarrow {}^{Z}Mg^{2+} + {}^{W}(OH)^{-}$.

381 A comparison of the three species is given in Table 10. Magnesio-lucchesiite also corresponds to

382 synthetic "oxy-uvite" investigated by Berryman et al. (2016).

383 The study of three samples of magnesio-lucchesiite shows the wide chemical variability

384 of this member of the tourmaline supergroup (Fig. 6). Indeed, whereas the holotype material is

385 Al-deficient, with 5.33 Al apfu, the synthetic "oxy-uvite" has 6.46 Al apfu (including 0.12 ^{T}Al

386 apfu; Berryman et al. 2016), and the sample #1 from San Piero in Campo is exceptionally

enriched in Al, with up to 7.74 Al apfu and 0.95 ^{T}Al apfu. The occurrence of ~1 Al apfu at the *T* site was previously reported only in adachiite, ideally $^{X}Ca^{Y}Fe^{2+}{}_{3}{}^{Z}Al_{6}{}^{T}(AlSi_{5})O_{18}(BO_{3})_{3}{}^{V}(OH)_{3}{}^{W}(OH)$ (Nishio-Hamane et al. 2014). Sample #1 is related to adachiite through the coupled substitution $^{T}Si^{4+} + {}^{W}O^{2-} = {}^{T}Al^{3+} + {}^{W}(OH)^{-}$, and its high ^{T}Al content is related to the high ^{Y}Al content, according to the heterovalent substitution $^{Y}Mg^{2+} + {}^{T}Si^{4+} = {}^{Y}Al^{3+} + {}^{T}Al^{3+}$. It is worth noting that sample #2 was collected in the same locality (but not in the same vein) as sample #1. It shows a higher proportion of magnesio-lucchesiite in its solid solution, with minor ^{T}Al and a partial substitution of ^{Z}Al by Fe^{3+}, confirming the existence of series with the uvite composition, ideally $^{X}Ca^{Y}Mg_{3}{}^{Z}(MgAl_{5})^{T}(AlSi_{5})O_{18}(BO_{3})_{3}{}^{V}(OH)_{3}{}^{W}(OH)$, reported by Scribner et al. (2017).The three magnesio-lucchesiite samples also contain strikingly variable contents of TiO_2 (1.92 vs. 0.00 vs. 0.78 wt.%). High contents of TiO_2 have been correlated with Al-deficient tourmalines with Mg disordered between *Y*- and *Z*-sites with elevated contents of Fe^{3+}. Many of the Ti-rich tourmalines are calcic but there is no limitation in terms of the Ca/Na ratio (Scribner et al. 2018; Gadas et al. 2019) as showed by the recent discovered of dutrowite, ideally $^{X}Na^{Y}(Fe^{2+}{}_{2.5}Ti_{0.5})^{Z}Al_{6}(Si_{6}O_{18})(BO_{3})_{3}(OH)_{3}O$ (Biagioni et al. 2020) The magnesio-lucchesiite occurrences are consistent with the incompatibility of Ti with high Al in tourmaline. Scribner et al. (2018) suggested that the behavior is caused by the small ionic radius of the Ti^{4+} cation (compared to relatively large cations such as Fe^{2+}, Mg^{2+}, and Fe^{3+}) which may partially reduce strain in the tourmaline structure caused by lack of Al^{3+}.

The smaller unit cell volume of the cotype material likely reflects the increased incorporation of the relatively small Al cation in the tourmaline structure compared to the holotype material. In this regard, Bosi et al. (2010) showed that the total content of Al is inversely correlated with the unit-cell volume. This correlation can hence explain the different

values of the unit cell volume and total Al of the cotype (V = 1566 Å^3 and Al = 7.7 apfu) and holotype (V = 1599 Å^3 and Al = 5.3 apfu) materials; this is supported by the synthetic "oxy-uvite" with Al = 6.46 apfu and intermediate unit-cell volume (V = 1573 Å^3; Berryman et al. 2016).

Implications

Magnesio-lucchesiite has been discovered at two localities, both of which are associated with Ca- and Mg-bearing ultrabasic rocks metasomatized by B-rich fluids. This association is rather unusual and, as the new tourmaline is black in color, it may be commonly overlooked or mistaken for a common black schorl or amphibole. At both occurrences, magnesio-lucchesiite contains an appreciable amount of Fe^{3+} and seems to form in oxidized conditions due to hydrothermal overprint of (ultra)basic rocks. However, a third occurrence of magnesio-lucchesiite was recently reported by Krmíček et al. (2020) from a calcite-dolomite marble in Černá (South Bohemia, Czech Republic). Magnesio-lucchesiite associated with fluor-uvite is a part of marble-hosted assemblage (Cal>Dol, Kfs, Pl, Tur, Ep, Ap) formed by a regional metamorphism of a calc-silicate rocks with evaporite component. This occurrence shows that stability of magnesio-lucchesiite is not restricted to replacement of amphibole and that it may also form by fluctuations of F and Al during crystallization of common uvitic tourmaline.

Current compositional data on magnesio-lucchesiite show that it forms an extensive solid solution with fluor-uvite, uvite, feruvite, fluor-feruvite and lucchesiite (Scribner et al. 2017), and at least partial solid solution with adachiite (this work) and dravite (Krmíček et al. 2020). Therefore, it has rather large petrogenetic potential, especially in Mg,Al-rich calcsilicate rocks, as well as contact-metamorphic, and metasomatic rocks.

Acknowledgments

This manuscript greatly benefited from constructive reviews by Eleanor J. Berryman and Darrell J. Henry. The authors thank Ronald Peterson and Brad Wilson for aiding in field work to collect the samples. The assistance of Valentina Dottorini during the preliminary characterization of the samples from Elba Island is acknowledged. The research was supported by NSERC Discovery Grant RGPIN-2015-06434 for L.A.G. and research project GAČR 17-17276S for J.C. Funding by Sapienza University of Rome (Prog. Università 2018 to F. Bosi) is gratefully acknowledged.

References

Anderson, R.G. (1983) Selwyn plutonic suite and its relationship to tungsten skarn mineralization, southeastern Yukon and District of Mackenzie. *In* Current Research, Part B. (Geological Survey of Canada, Paper 83-1B). Ottawa, Ontario, Minister of Supply and Services Canada (151–163).

Andreozzi, G.B., Bosi, F., and Longo, M. (2008) Linking Mössbauer and structural parameters in elbaite-schorl-dravite tourmalines. American Mineralogist, 93, 658–666.

Bačík, P., Cempírek, J., Uher, P., Novák, M., Ozdín, D., Filip, J., Škoda, R., Breiter, K., Klementová, M., Ďuďa, R., and Groat, L.A. (2013) Oxy-schorl, $Na(Fe^{2+}_2Al)Al_6Si_6O_{18}(BO_3)_3(OH)_3O$, a new mineral from Zlatá Idka, Slovak Republic and Přibyslavice, Czech Republic. American Mineralogist, 98, 485–492.

455 Barboni, M., Annen, C., and Schoene, B. (2015) Evaluating the construction and evolution of
456 upper crustal magma reservoirs with coupled U/Pb zircon geochronology and thermal
457 modeling: A case study from the Mt. Capanne pluton (Elba, Italy). Earth and Planetary
458 Science Letters, 432, 436–448.
459 Berryman, E.J., Wunder, B., Ertl, A., Koch-Müller, M., Rhede, D., Scheidl, K., Giester, G., and
460 Heinrich, W. (2016) Influence of the X-site composition on tourmaline's crystal
461 structure: investigation of synthetic K-dravite, dravite, oxy-uvite, and magnesio-foitite
462 using SREF and Raman spectroscopy. Physics and Chemistry of Minerals, 43, 83–102.
463 Biagioni, C., Bosi, F., Mauro, D., Skogby, H., Dini, A., and Zaccarini, F. (2020) Dutrowite, IMA
464 2019-082, in: CNMNC Newsletter 53, European Journal of Mineralogy 32,
465 https://doi.org/10.5194/ejm-32-209-2020, 2020.
466 Bosi, F. (2013) Bond-valence constraints around the O1 site of tourmaline. Mineralogical
467 Magazine, 77, 343–351.
468 Bosi, F. (2018) Tourmaline crystal chemistry. American Mineralogist, 103, 298–306.
469 Bosi, F., and Lucchesi, S. (2007) Crystal chemical relationships in the tourmaline group:
470 Structural constrains on chemical variability. American Mineralogist, 92, 1054–1063.
471 Bosi, F., Balić-Žunić, T., and Surour, A.A. (2010) Crystal structure analysis of four tourmalines
472 from the Cleopatra's Mines (Egypt) and Jabal Zalm (Saudi Arabia), and the role of Al in
473 the tourmaline group. American Mineralogist, 95, 510–518.
474 Bosi, F., Skogby, H., Lazor, P., and Reznitskii, L. (2015) Atomic arrangements around the O3
475 site in Al- and Cr-rich oxy-tourmalines: a combined EMP, SREF, FTIR and Raman
476 study. Physics and Chemistry of Minerals, 42, 441–453.

Bosi, F., Skogby, H., Ciriotti, M.E., Gadas, P., Novák, M., Cempírek, J., Všianský, D., and Filip, J. (2017a) Lucchesiite, $CaFe^{2+}_3Al_6(Si_6O_{18})(BO_3)_3(OH)_3O$, a new mineral species of the tourmaline supergroup. Mineralogical Magazine, 81, 1–14.

Bosi F, Reznitskii L, Hålenius U., and Skogby H (2017b) Crystal chemistry of Al-V-Cr oxy-tourmalines from Sludyanka complex, Lake Baikal, Russia. European Journal of Mineralogy, 29, 457–472.

Bosi F., Biagioni C., and Oberti R. (2019a) On the chemical identification and classification of minerals. Minerals, 9, 591.

Bosi, F., Hatert, F., Hålenius, U., Pasero, M., Miyawaki, R., and Mills, S.J. (2019b) On the application of the IMA-CNMNC dominant-valency rule to complex mineral compositions. Mineralogical Magazine, 83, 627–632.

Bosi, F., Pezzotta, F., Altieri, A., Andreozzi, G. B., Ballirano, P., and Tempesta, G. (2020a) Celleriite, IMA 2019-089, in: CNMNC Newsletter 53, European Journal of Mineralogy, 32, https://doi.org/10.5194/ejm-32-209-2020, 2020.

Bosi, F., Biagioni, C., Pezzotta, F., Skobgy, H., Hålenius, U., Cempírek, J., Hawthorne, F.C., Lussier, A.J., Abdu, Y.A., Day, M.C., Fayek, M., Clark, C. M., Grice, J.D., and Henry, D.J. (2020b) Uvite, IMA 2019-113, in: CNMNC Newsletter 54, European Journal of Mineralogy, 32, https://doi.org/10.5194/ejm-32-275-2020, 2020.

Brown, I.D. (2002) The chemical bond in inorganic chemistry: The bond valence model. IUCr Monographs on Crystallography 12. Oxford University Press, Oxford, United Kingdom.

Brown, I.D., and Altermatt, D. (1985) Bond-valence parameters obtained from a systematic analysis of the Inorganic Crystal Structure Database. Acta Crystallographica, B41, 244–247.

500 Bruker (2007) SAINT. Bruker AXS Inc., Madison, Wisconsin.

501 Creagh, D.C., and Hubbell, J.H. (1992) International Tables for Crystallography (Vol. C) pp.
502 200–206. Kluwer, Boston.

503 Creagh, D.C., and McAuley, W.J. (1992) International Tables for Crystallography (Vol. C) pp.
504 219–222. Kluwer, Boston.

505 Cromer, D.T., and Waber, J.T. (1974) International Tables for X-ray Crystallography (Vol. IV)
506 The Kynoch Press, Birmingham, England.

507 Dini, A., Innocenti, F., Rocchi, S., Tonarini, S., and Westerman D.S. (2002) The magmatic
508 evolution of the late Miocene laccolith–pluton–dyke granitic complex of Elba Island,
509 Italy. Geological Magazine, 139, 257–279.

510 Dutrow, B.L., and Henry, D.J. (2011) Tourmaline: a geologic DVD. Elements, 7, 301–306.

511 Ercit, T.S., Groat, L.A., and Gault, R.A. (2003) Granitic pegmatites of the O'Grady batholith,
512 N.W.T., Canada: a case study of the evolution of the elbaite subtype of rare-element
513 granitic pegmatite. The Canadian Mineralogist, 41, 117–137.

514 Ertl, A., Henry, D. J., and Tillmanns, E. (2018) Tetrahedral substitutions in tourmaline: a review.
515 European Journal of Mineralogy, 30, 465–470.

516 Farina, F., Stevens, G., Dini, A., and Rocchi, S. (2012) Peritectic phase entrainment and magma
517 mixing in the late Miocene Elba Island laccolith–pluton–dyke complex (Italy). Lithos,
518 153, 243–260.

519 Gadas, P., Novák, M., Cempírek, J., Filip, J., Vašinová–Galiová, M., Groat, L.A., and Všianský,
520 D. (2014) Mineral assemblages, compositional variation, and crystal structure of feruvitic
521 tourmaline from a contaminated anatectic pegmatite at Mirošov near Strážek,
522 Moldanubian Zone, Czech Republic. The Canadian Mineralogist, 52, 285–301.

523 Gonzalez-Carreño, T., Fernández, M., and Sanz, J. (1988) Infrared and electron microprobe
524 analysis of tourmaline. Physics and Chemistry of Minerals, 15, 452–460.
525 Gordey, S.P. and Anderson, R.G. (1993) Evolution of the northern Cordilleran miogeocline,
526 Nahanni map area (105I), Yukon and Northwest Territories. *Geological Survey of*
527 *Canada: Memoir 428*, Canada Communications Group, Ottawa, Ontario Canada.
528 Grice, J.D., and Robinson, G.W. (1989) Feruvite, a new member of the tourmaline group, and its
529 crystal structure. The Canadian Mineralogist, 27, 199–203.
530 Henry, D.J., Novák, M., Hawthorne, F.C., Ertl, A., Dutrow, B.L., Uher, P., and Pezzotta, F.
531 (2011) Nomenclature of the tourmaline-supergroup minerals. American Mineralogist, 96,
532 895–913.
533 Hunt, P.A., and Roddick, J.C. (1987) A compilation of K–Ar ages. *In* Radiogenic age and
534 Isotopic studies: Report 1. Canadian Government Publishing Centre, Ottawa, Ontario
535 (895–913).
536 Ibers, J.A., and Hamilton, W.C. (1964) Dispersion corrections and crystal structure refinements.
537 Acta Crystallographica, 17, 781–782.
538 Krmíček, L., Novák, M., Trumbull, R.B., Cempírek, J., and Houzar, S. (2020) Boron isotopic
539 variations in tourmaline from metacarbonates and associated calc-silicate rocks from the
540 Bohemian Massif: a first study constraints on boron recycling in the Variscan orogen.
541 Geoscience Frontiers (in press).
542 https://doi.org/10.1016/j.gsf.2020.03.009
543 Mattson, S.M., and Rossman, G.R. (1987) Fe^{2+}–Fe^{3+} interactions in tourmaline. Physics and
544 Chemistry of Minerals, 14, 163–171.

545 Merlet, C. (1994) An accurate computer correction program for quantitative electron-probe
546 microanalysis. Microchimica Acta, 114, 363–376.
547 Nishio-Hamane, D., Minakawa, T., Yamaura, J., Oyama, T., Ohnishi, M., and Shimobayashi, N.
548 (2014) Adachiite, a Si-poor member of the tourmaline supergroup from the Kiura mine,
549 Oita Prefecture, Japan. Journal of Mineralogical and Petrological Sciences, 109, 74–78.
550 Pouchou, J.L., and Pichoir, F. (1991) Quantitative analysis of homogeneous or stratified
551 microvolumes applying the model "PAP." Pp. 3l–75 in: Electron Probe Quantitation
552 (K.F.J. Heinrich and D.E. Newbury, editors). Plenum Press, New York.
553 Prescher, C., McCammon, C., and Dubrovinsky, L. (2012) MossA: a program for analyzing
554 energy-domain Mössbauer spectra from conventional and synchrotron sources. Journal of
555 Applied Crystallography, 45, 329–331.
556 Robert, J.-L., Gourdant, J.P., Linnen, R.L., Rouer, O. and Benoist, P. (1997) Crystal-chemical
557 relationships between OH, F and Na in tourmalines. In Tourmaline 1997, Int. Symp. on
558 Tourmaline, (Nove Mesto na Morave), Abstr., 84.
559 Scribner, E.D., Groat, L.A., and Cempírek, J. (2018) Mineralogy of Ti-bearing, Al-deficient
560 tourmaline assemblages associated with lamprophyre dikes near the O'Grady Batholith,
561 Northwest Territories, Canada. Journal of Geosciences, 63, 123–135.
562 Sheldrick, G.M. (1996) SADABS. University of Göttingen, Germany.
563 Sheldrick, G.M. (2015) Crystal structure refinement with SHELXL. Acta Crystallographica,
564 C71, 3–8.
565 Skogby, H., Bosi, F., and Lazor, P. (2012) Short-range order in tourmaline: a vibrational
566 spectroscopic approach to elbaite. Physics and Chemistry of Minerals, 39, 811–816.

567 Slack, J.F., and Trumbull, R.B. (2011) Tourmaline as a Recorder of Ore-Forming Processes.
568 Elements, 7, 321–326.
569 Smith, G. (1978) A reassessment of the role of iron in the 5,000 - 30,000 cm^{-1} region of the
570 electronic absorption spectra of tourmaline. Physics and Chemistry of Minerals, 3, 343–
571 373.
572 Spek, A.L.J. (2003) Single-crystal structure validation with the program PLATON. *Journal of*
573 Applied Crystallography, 36, 7–13.
574 Taran, M.N., Lebedev, A.S., and Platonov, A.N. (1993) Optical absorption spectroscopy of
575 synthetic tourmalines. Physics and Chemistry of Minerals, 20, 209–220.
576 Tonarini, S., Dini, A., Pezzotta, F., and Leeman, W.P. (1998) Boron isotopic composition of
577 zoned (schorl-elbaite) tourmalines, Mt. Capanne Li-Cs pegmatites, Elba (Italy). European
578 Journal of Mineralogy, 10, 941–951.
579 van Hinsberg, V.J., Henry, D.J., and Marschall, H.R. (2011) Tourmaline: an ideal indicator of its
580 host environment. The Canadian Mineralogist, 49, 1–16.
581

This is the peer-reviewed, final accepted version for American Mineralogist, published by the Mineralogical Society of America.
The published version is subject to change. Cite as Authors (Year) Title. American Mineralogist, in press.
DOI: https://doi.org/10.2138/am-2021-7496. http://www.minsocam.org/

582 TABLES

583

584 Table 1: EMPA data for holotype magnesio-lucchesiite from O'Grady Batholith, Canada.

Constituent	Mean (n = 2)	Range	σ
P_2O_5 (wt. %)	b.d.	b.d.	b.d.
SiO_2	35.23	35.05-35.42	0.18
TiO_2	1.92	1.88-1.96	0.04
$B_2O_{3\ calc}$*	10.23		
Al_2O_3	26.63	26.62-26.65	0.02
V_2O_3	0.08	0.08-0.08	0.00
Cr_2O_3	0.10	0.09-0.12	0.01
Fe_2O_3†	6.14		
FeO†	4.34		
FeO_{tot}	9.87	9.86-9.89	0.02
MnO	b.d.	b.d.	b.d.
ZnO	b.d.	b.d.	b.d.
MgO	7.96	7.92-8.00	0.04
CaO	3.27	3.24-3.31	0.03
Na_2O	1.19	1.17-1.20	0.02
K_2O	0.04	0.03-0.05	0.01
F	0.41	0.36-0.47	0.05
Cl	b.d.	b.d.	b.d.
$H_2O_{\ calc}$‡	2.29		
-(O=F)	-0.17	(-0.20) - (-0.15)	0.02
Total	99.67	99.43-99.82	0.19

585 *B_2O_3 fixed at 3 *apfu* B; †Fe_2O_3 and FeO were calculated as described in the EMPA subsection of
586 Analytical Methods and Results; ‡H_2O content calculated based on stoichiometry; b.d. = below detection
587 limit
588

This is the peer-reviewed, final accepted version for American Mineralogist, published by the Mineralogical Society of America.
The published version is subject to change. Cite as Authors (Year) Title. American Mineralogist, in press.
DOI: https://doi.org/10.2138/am-2021-7496. http://www.minsocam.org/

589 Table 2: EMPA data for two samples of cotype magnesio-lucchesiite from San Piero in Campo,
590 Elba, Italy.

Constituent	Sample #1			Sample #2		
	Mean (n = 16)	Range	σ	Mean (n = 7)	Range	σ
SiO_2	30.26	29.65-30.73	0.34	35.10	34.06-35.75	0.66
TiO_2	b.d.			0.78	0.42-1.15	0.35
$B_2O_{3\ calc}$*	10.41			10.39		
Al_2O_3	39.30	37.40-40.53	0.98	28.29	27.21-30.38	1.33
V_2O_3	b.d.			0.10	0.05-0.14	0.03
$Fe_2O_3^{\dagger}$	2.86			3.66		
$FeO^{\dagger}$	2.90			2.92		
FeO_{tot}	5.47	4.48-6.86	0.81	6.22	5.23-7.29	0.88
MgO	5.82	5.42-6.19	0.23	10.35	10.07-10.63	0.21
CaO	4.93	4.78-5.02	0.07	3.98	3.68-4.22	0.20
Na_2O	0.37	0.32-0.41	0.03	0.66	0.58-0.71	0.06
K_2O	b.d.			b.d.		
F	0.04	0-0.07	0.03	b.d.		
$H_2O_{calc}^{\ddagger}$	2.60			3.04		
-(O=F)	-0.02			-		
Total	99.47					

591 *B_2O_3 fixed at 3.000 *apfu* B; $^{\dagger}Fe_2O_3$ and FeO were determined by Mössbauer spectroscopy as described
592 in the Mössbauer spectroscopy subsection of Analytical Methods and Results; $^{\ddagger}H_2O$ content calculated
593 based on stoichiometry, under the assumption of (Y+Z+T) = 15.000 apfu; b.d. = below detection limit
594

This is the peer-reviewed, final accepted version for American Mineralogist, published by the Mineralogical Society of America.
The published version is subject to change. Cite as Authors (Year) Title. American Mineralogist, in press.
DOI: https://doi.org/10.2138/am-2021-7496. http://www.minsocam.org/

595 Table 3: Mössbauer hyperfine parameters for fitted quadrupole doublets for cotype magnesio-
596 lucchesiite from San Piero in Campo, Elba, Italy.

597

Site	Sample #1				Sample #2			
	CS (mm/s)	QS (mm/s)	FWHM (mm/s)	I(%)	CS (mm/s)	QS (mm/s)	FWHM (mm/s)	I(%)
$^{VI}Fe^{2+}$ (*Y*1)	1.07	2.53	0.34	13	1.08	2.58	0.34	9
$^{VI}Fe^{2+}$ (*Y*2)	1.02	2.14	0.38	23	1.06	2.31	0.38	12
$^{VI}Fe^{2+}$ (*Y*3)	1.03	1.59	0.38	17	0.97	1.80	0.38	26
$^{VI}Fe^{3+}$	0.46	0.89	0.65	47	0.41	0.82	0.65	53

598 CS = Centroid shift; QS = Quadrupole splitting; FWHM = Full width at half maximum; I = Relative area of
599 absorption.
600

This is the peer-reviewed, final accepted version for American Mineralogist, published by the Mineralogical Society of America.
The published version is subject to change. Cite as Authors (Year) Title. American Mineralogist, in press.
DOI: https://doi.org/10.2138/am-2021-7496. http://www.minsocam.org/

601 Table 4: Single crystal XRD data and refinement information for magnesio-lucchesiite from
602 O'Grady Batholith, Canada (holotype) and San Piero in Campo, Italy (cotype).

	Canada	Italy sample #1
a (Å)	15.9910(3)	15.9270(10)
c (Å)	7.2224(2)	7.1270(5)
V (Å^3)	1599.42(7)	1565.7(2)
Space group	$R3m$	$R3m$
Z	3	3
Crystal size (μm)	49 × 125 × 136	25 × 30 × 70
Radiation	Mo $K\alpha$	Mo $K\alpha$
Monochromator	graphite	graphite
2θ (°)	5.2–91	5.12–63.11
Total F_o	21660	9398
Unique F_o	3214	1273
$F_o > 4\sigma F_o$	2953	1225
R_{int}, $R\sigma$	0.0422, 0.0330	0.0502, 0.0327
Refined parameters	95	93
Range of h	-30 ≤ 32	-23 ≤ 22
Range of k	-30 ≤ 31	-23 ≤ 23
Range of l	-14 ≤ 14	-10 ≤ 10
R_1 for $F_o > 4\sigma F_o$	0.0306	0.0196
R_1 for all unique F_o	0.0356	0.0211
wR_2	0.0575	0.0416
GooF (=S)	1.052	1.071
$\Delta\rho_{max}$ (e Å^{-3})	1.108	0.31
$\Delta\rho_{min}$ (e Å^{-3})	-1.103	-0.44

603

This is the peer-reviewed, final accepted version for American Mineralogist, published by the Mineralogical Society of America.
The published version is subject to change. Cite as Authors (Year) Title. American Mineralogist, in press.
DOI: https://doi.org/10.2138/am-2021-7496. http://www.minsocam.org/

Table 5: Fractional atomic coordinates and isotropic (U_{iso}) or equivalent isotropic (U_{eq}) displacement parameters (in Å^2) for magnesio-luccesiite from O'Grady Batholith, Canada (holotype) and San Piero in Campo, Elba, Italy (cotype).

Sites	Canada sample				Italy sample #1			
	x/*a*	*y*/*b*	*z*/*c*	U_{eq}/U_{iso}	*x*/*a*	*y*/*b*	*z*/*c*	U_{eq}/U_{iso}
X	0	0	0.22443(18)	0.0133(4)	0	0	0.2089(2)	0.0158(5)
Y	0.12382(3)	0.06191(2)	0.63488(8)	0.00770(13)	0.12200(7)	0.06100(3)	0.63936(16)	0.0062(3)
Z	0.29840(3)	0.26182(3)	0.61227(9)	0.00463(11)	0.29730(5)	0.26122(5)	0.60775(15)	0.0056(2)
T	0.19180(3)	0.19009(3)	0	0.00404(8)	0.19229(5)	0.19039(5)	0	0.00578(15)
B	0.11011(8)	0.22022(17)	0.4530(3)	0.0060(3)	0.10924(15)	0.2185(3)	0.4480(5)	0.0058(7)
O(1)	0.0000	0.0000	0.7804 (5)	0.0158 (6)	0	0	0.7719(7)	0.0155(10)
O(2)	0.06067 (6)	0.12135 (12)	0.4769 (3)	0.0103 (3)	0.05970(9)	0.11939(18)	0.4775(4)	0.0093(5)
O(3)	0.26733 (14)	0.13367 (7)	0.5124 (2)	0.0111 (3)	0.2623(2)	0.13114(10)	0.5057(4)	0.0099(5)
O(4)	0.09198 (6)	0.18395 (13)	0.0712 (2)	0.0090 (3)	0.09229(11)	0.1846(2)	0.0753(4)	0.0137(6)
O(5)	0.18194 (13)	0.09097 (7)	0.0912 (2)	0.0090 (2)	0.1821(2)	0.09104(11)	0.0970(4)	0.0134(6)
O(6)	0.19612 (8)	0.18711 (8)	0.77865 (16)	0.00776 (17)	0.19478(12)	0.18424(12)	0.7727(3)	0.0069(3)
O(7)	0.28462 (8)	0.28410 (8)	0.08063 (16)	0.00769 (17)	0.28744(12)	0.28615(12)	0.0768(2)	0.0070(4)
O(8)	0.20926 (8)	0.26982 (9)	0.44201 (18)	0.00909 (18)	0.20852(12)	0.26899(13)	0.4356(3)	0.0068(4)
H(3)	0.262 (3)	0.1312 (17)	0.403 (7)	0.026 (12)	0.244(3)	0.1222(15)	0.376(4)	0.01185

This is the peer-reviewed, final accepted version for American Mineralogist, published by the Mineralogical Society of America.
The published version is subject to change. Cite as Authors (Year) Title. American Mineralogist, in press.
DOI: https://doi.org/10.2138/am-2021-7496. http://www.minsocam.org/

608 Table 6: Site populations based on single crystal XRD, and refined and calculated site scattering
609 values in magnesio-lucchesiite from O'Grady Batholith, Canada (holotype) and San Piero in
610 Campo, Elba, Italy (cotype).

611
612

Site	Sample	Site population (apfu)	Site scattering (electron pfu)	613
			Calculated	Refined
X	Canada	$Ca_{0.60}Na_{0.39}K_{0.01}$	16.38	16.06(27)
	Italy sample #1	$Ca_{0.88}Na_{0.12}$	18.92	19.15(36)
Y	Canada	$Mg_{1.27}Fe^{2+}_{0.62}Fe^{3+}_{0.61}Ti_{0.25}Al_{0.23}V_{0.01}Cr_{0.01}$	56.17	56.11(14)
	Italy sample #1	$Al_{1.43}Fe^{3+}_{0.19}Mg_{0.98}Fe^{2+}_{0.40}$	45.68	45.73(27)
Z	Canada	$Al_{5.08}Fe^{3+}_{0.17}Mg_{0.75}$	79.49	79.38(8)
	Italy sample #1	$Al_{5.36}Fe^{3+}_{0.17}Mg_{0.47}$	79.79	79.86(60)
T	Canada	$Si_{5.98}Al_{0.02}$	83.98	84*
	Italy sample #1	$Si_{5.05}Al_{0.95}$	83.05	84*

614 *Fixed in the final stages of refinement.

This is the peer-reviewed, final accepted version for American Mineralogist, published by the Mineralogical Society of America.
The published version is subject to change. Cite as Authors (Year) Title. American Mineralogist, in press.
DOI: https://doi.org/10.2138/am-2021-7496. http://www.minsocam.org/

615 Table 7: Selected bond lengths (Å) in magnesio-lucchesiite from O'Grady Batholith, Canada
616 (holotype) and San Piero in Campo, Elba, Italy (cotype).

617

		Canada	Italy sample #1
X	–O(2) (×3)	2.4799(19)	2.526(3)
	–O(5) (×3)	2.6971(18)	2.635(3)
	–O(4) (×3)	2.7774(18)	2.718(3)
	mean	2.6515	2.626
Y	–O(1)	2.0112(19)	1.930(2)
	–O(6) (×2)	2.0270(12)	1.9554(19)
	–O(2) (×2)	2.0455(12)	2.0255(19)
	–O(3)	2.175(2)	2.156(3)
	mean	2.0553	2.008
Z	–O(6)	1.8953(12)	1.8838(18)
	–O(8)	1.9027(12)	1.9007(18)
	–O(7)	1.9077(12)	1.8858(18)
	–O(8)	1.9346(13)	1.9223(19)
	–O(7)	1.9728(12)	1.9325(18)
	–O(3)	1.9871(9)	1.9943(13)
	mean	1.9333	1.9199
B	–O(8) (×2)	1.3754(16)	1.372(3)
	–O(2)	1.380(3)	1.383(5)
	mean	1.3770	1.376
T	–O(6)	1.6019(12)	1.625(2)
	–O(7)	1.6034(11)	1.6160(18)
	–O(4)	1.6328(7)	1.6389(11)
	–O(5)	1.6496(8)	1.6584(13)
	mean	1.6219	1.634

618

This is the peer-reviewed, final accepted version for American Mineralogist, published by the Mineralogical Society of America.
The published version is subject to change. Cite as Authors (Year) Title. American Mineralogist, in press.
DOI: https://doi.org/10.2138/am-2021-7496. http://www.minsocam.org/

619 Table 8: Bond-valence (BV) table for the structural formula of magnesio-lucchesiite from
620 O'Grady Batholith, Canada (holotype).

	X	***Y***	***Z***	***B***	***T***	**Σ BV**
O(1)*		$0.433^{\times 3}\rightarrow$				1.300
O(2)	$0.215^{\times 3}\downarrow$	$0.420^{\times 2}\downarrow\rightarrow$		0.976		2.030
O(3)*		0.296	$0.413^{\times 2}\rightarrow$			1.122
O(4)	$0.096^{\times 3}\downarrow$				$0.977^{\times 2}\rightarrow$	2.049
O(5)	$0.119^{\times 3}\downarrow$				$0.933^{\times 2}\rightarrow$	1.986
O(6)		$0.441^{\times 2}\downarrow$	0.529		1.062	2.033
O(7)			0.512		1.057	1.999
			0.429			
O(8)			0.519	$0.988^{\times 2}\downarrow$		1.983
			0.476			
Σ BV	1.290	2.452	2.879	2.952	4.029	
IC(avg)	1.591	2.452	2.876	3.000	3.997	
Δ	0.301	0.000	-0.004	0.048	-0.032	
**hydrogen bond donor*						
IC(avg) = average formal charge of atoms occupying the site						

621

This is the peer-reviewed, final accepted version for American Mineralogist, published by the Mineralogical Society of America.
The published version is subject to change. Cite as Authors (Year) Title. American Mineralogist, in press.
DOI: https://doi.org/10.2138/am-2021-7496. http://www.minsocam.org/

Table 9. Calculated X-ray powder diffraction data (*d* in Å) for magnesio-lucchesiite from O'Grady Batholith, Canada (holotype).

d_{calc}	I_{obs}*	I_{calc}	*hkl*		d_{calc}	I_{obs}*	I_{calc}	*hkl*
7.995	4	3	1 1 0		1.570	2	2	3 2 4
6.404	**32**	**31**	**1 0 1**		1.551	3	4	4 6 1
4.998	17	17	0 2 1		1.539	4	4	9 0 0
4.616	21	20	0 3 0		1.532	5	5	7 2 2
4.238	**54**	**53**	**2 1 1**		1.513	15	16	0 5 4
3.998	**58**	**55**	**2 2 0**		1.511	4	3	8 2 0
3.494	**46**	**44**	**0 1 2**		1.486	4	4	2 4 4
3.391	6	6	1 3 1		1.479	2	2	1 8 2
3.022	12	12	4 1 0		1.461	16	16	5 1 4
2.972	**70**	**67**	**1 2 2**		1.459	5	5	1 7 3
2.908	11	11	3 2 1		1.454	5	5	6 4 2
2.631	5	5	3 1 2		1.437	5	4	0 1 5
2.586	**100**	**100**	**0 5 1**		1.436	6	6	7 4 0
2.499	4	3	0 4 2		1.423	8	7	6 5 1
2.461	4	4	2 4 1		1.415	9	10	4 3 4
2.407	8	7	0 0 3		1.413	5	5	6 3 3
2.385	14	14	2 3 2		1.360	10	10	10 0 1
2.352	14	13	5 1 1		1.347	4	4	5 6 2
2.308	3	3	6 0 0		1.334	4	4	3 5 4
2.218	2	2	5 2 0		1.333	6	6	6 6 0
2.198	13	13	5 0 2		1.332	5	5	5 5 3
2.171	14	12	4 3 1		1.315	3	3	2 3 5
2.135	12	11	3 0 3		1.314	10	10	1 10 0
2.119	5	5	4 2 2		1.310	3	3	8 3 2
2.062	14	13	2 2 3		1.293	2	2	0 10 2
2.048	**46**	**43**	**1 5 2**		1.288	2	2	8 4 1
2.027	9	9	1 6 1		1.281	11	11	5 0 5
1.999	5	5	4 4 0		1.280	6	7	2 8 3
1.926	29	26	3 4 2		1.265	3	3	5 4 4
1.908	0	2	3 5 1		1.240	4	4	0 11 1
1.883	7	6	1 4 3		1.233	2	2	7 4 3
1.856	8	8	6 2 1		1.230	2	2	4 8 2
1.823	1	2	6 1 2		1.220	2	2	3 4 5
1.787	4	4	3 3 3		1.204	2	2	0 0 6
1.747	2	2	0 2 4		1.185	4	4	11 1 1

This is the peer-reviewed, final accepted version for American Mineralogist, published by the Mineralogical Society of America.
The published version is subject to change. Cite as Authors (Year) Title. American Mineralogist, in press.
DOI: https://doi.org/10.2138/am-2021-7496. http://www.minsocam.org/

1.735	0	2	0 7 2		1.165	2	2	3 0 6
1.696	4	4	2 6 2		1.159	2	2	10 3 1
1.666	20	19	0 6 3		1.154	5	6	10 1 3
1.647	13	13	2 7 1		1.139	0	2	1 11 2
1.601	4	3	4 0 4		1.131	2	2	1 9 4
1.599	19	19	5 5 0		1.130	2	3	9 3 3
1.592	4	4	4 5 2		1.099	3	3	10 0 4
1.582	2	2	8 1 1					

Note: Bold – strongest reflections. Lines with I_{calc} less than 2 are not shown.
*I_{obs} values were generated from the observed single-crystal XRD intensities whereas I_{calc} are theoretical values calculated based on the observed structure.

624

This is the peer-reviewed, final accepted version for American Mineralogist, published by the Mineralogical Society of America.
The published version is subject to change. Cite as Authors (Year) Title. American Mineralogist, in press.
DOI: https://doi.org/10.2138/am-2021-7496. http://www.minsocam.org/

Table 10: Comparison of holotype magnesio-lucchesiite (O'Grady Batholith, Canada) formula and properties to some related tourmaline supergroup minerals.

		Magnesio-lucchesiite	Lucchesiite	Feruvite
Chemical formula	*X*	Ca	Ca	Ca
	Y_3	Mg_3	$Fe^{2+}{}_3$	$Fe^{2+}{}_3$
	Z_6	Al_6	Al_6	$MgAl_5$
	T_6O_{18}	Si_6O_{18}	Si_6O_{18}	Si_6O_{18}
	$(BO_3)_3$	$(BO_3)_3$	$(BO_3)_3$	$(BO_3)_3$
	V_3	$(OH)_3$	$(OH)_3$	$(OH)_3$
	W	O	O	(OH)
Crystal system		Trigonal	Trigonal	Trigonal
Space group		*R*3*m*	*R*3*m*	*R*3*m*
Unit-cell parameters		*a* = 15.9910(3) Å *c* = 7.2224(2) Å *V* = 1599.42(7) Å^3 Z = 3	*a* = 16.0018(7) Å *c* = 7.2149(3) Å *V* = 1599.92 Å^3 Z = 3	*a* = 16.012(2) Å *c* = 7.245(2) Å *V* = 1606.6(4) Å^3 Z = 3
Density (calc.) g/cm^3		3.168	3.209	3.207
Optical properties		Uniaxial (−) n_ω = 1.668 n_ε = 1.644	Uniaxial (−) n_ω = 1.670 n_ε = 1.655	Uniaxial (−) n_ω = 1.687 n_ε = 1.669
Pleochroism		O = dark brown E = colorless to dark brown	O = very dark brown E = light brown	O = light brown E = very dark brown
Reference		This work	Bosi et al. (2017a)	Grice and Robinson (1989)

Notes: Berryman et al. (2016) reported following unit-cell parameters for synthetic "oxy-uvite": *a* = 15.907(1) Å, *c* = 7.179(1) Å, and *V* = 1573.2(3) Å^3; The pleochroism reported in Grice and Robinson (1989) is anomalous. All other tourmalines reported so far in literature display a reverse pleochroic scheme with O > E.

633 FIGURE CAPTIONS

634

635 Fig. 1. Grain of magnesio-lucchesiite (dark brown) enclosed in uvitic tourmaline together with
636 dravite (Drv) at the contact of the lamprophyre dyke.

637

638 Fig. 2. Magnesio-lucchesiite as prismatic crystals, up to 3 mm in size (field of view ca. 15 mm),
639 with a chlorite-group mineral (a), and back-scattered electron image showing a slight
640 compositional zoning in a crystal fragment. The red dotted box indicates the area where the grain
641 used for structure refinement was obtained (b). San Piero in Campo, Elba Island, Livorno,
642 Tuscany, Italy. Sample #1. Museo di Storia Naturale, Università di Pisa, catalogue number
643 15921.

644

645 Fig. 3. Mössbauer spectra of magnesio-lucchesiite from San Piero in Campo: (a) sample #1 and
646 (b) sample #2.

647
648 Fig. 4. Infrared spectra of sample #1 (a) and #2 (b) of magnesio-lucchesiite from San Piero in
649 Campo.

650
651 Fig. 5. Polarized optical absorption spectra of samples #1 (a) and #2 (b) of magnesio-lucchesiite
652 from San Piero in Campo recorded at room temperature.

653

654 Fig. 6. Composition of magnesio-lucchesiite holotype from the O'Grady Batholith, Canada, two
655 crystals (co-type and sample #2) from co-type locality San Piero in Campo, Elba, Italy, and

656 synthetic "oxy-uvite" of Berryman et al. (2016). R^{3+} cations include Fe^{3+} and Al^{3+}. Luc =

657 Lucchesiite, Adc = Adachiite, Fuv = Feruvite, Uv = Uvite.

Figure 1


Lamprophyre dike
Drv
Uvite + Fluor-uvite
Magnesio-lucchesiite
Drv
Uvite
Uvite
Drv + Oxy-drv
Qz
Fe-oxide
1 mm

Figure 2

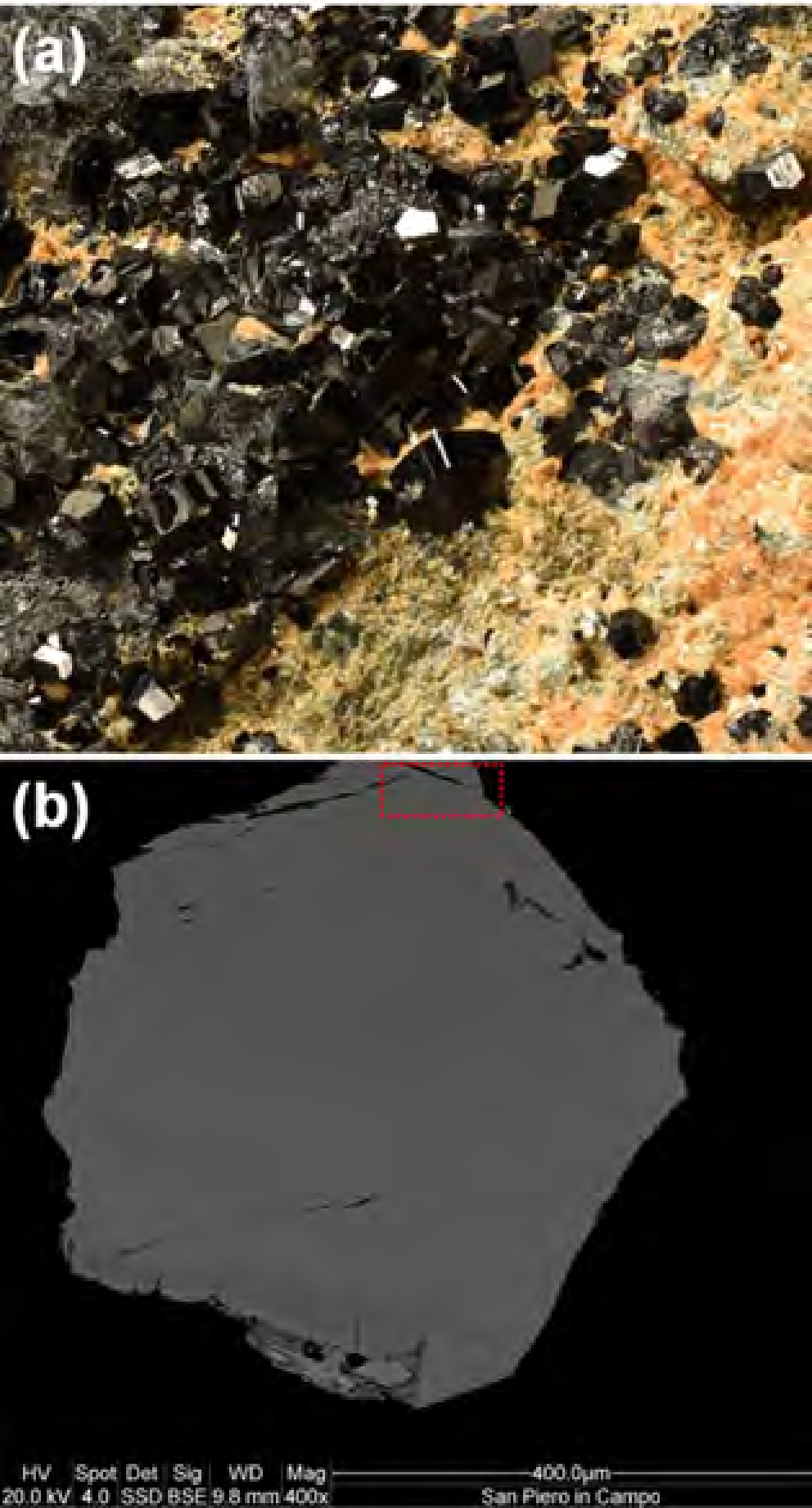
(a)
(b)
HV Spot Det Sig WD Mag
20.0 kV 4.0 SSD BSE 9.8 mm 400x
400.0µm
San Piero in Campo

Figure 3a

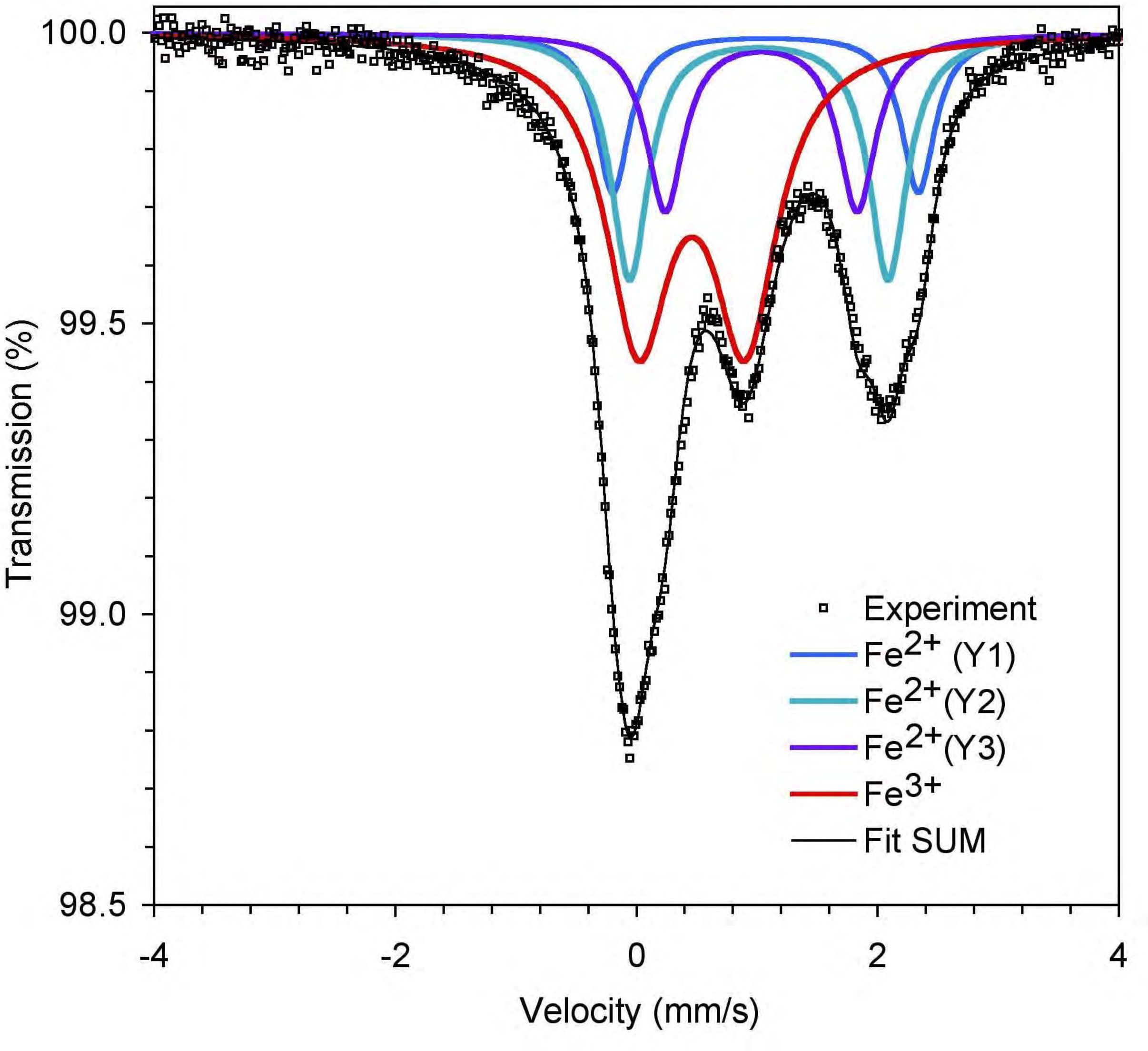
100.0
99.5
99.0
98.5
Transmission (%)
-4
-2
0
2
4
Velocity (mm/s)
Experiment
Fe2+ (Y1)
Fe2+(Y2)
Fe2+(Y3)
Fe3+
Fit SUM

Figure 3b

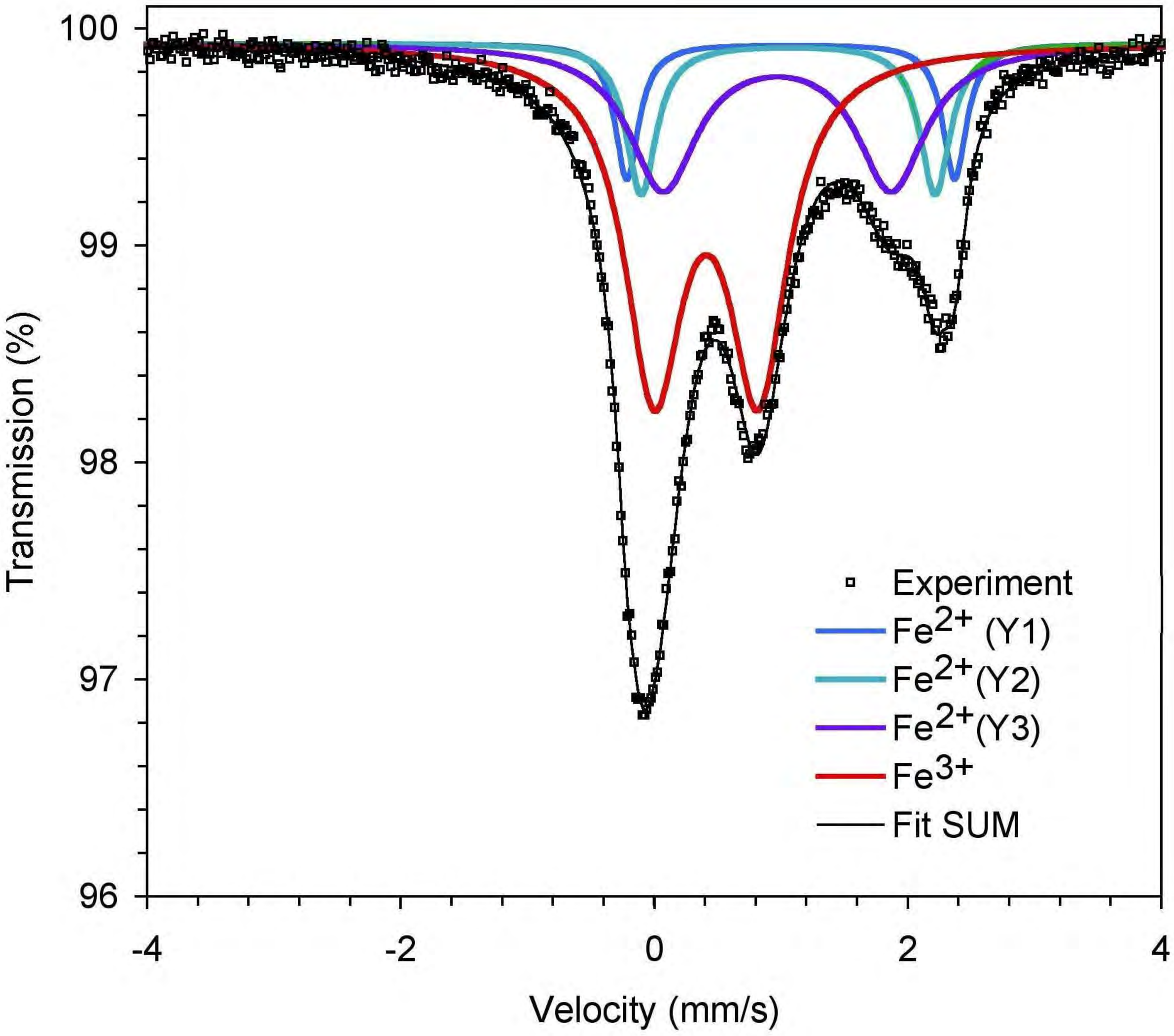
100
99
98
97
96
Transmission (%)
-4
-2
0
2
4
Velocity (mm/s)
Experiment
Fe2+ (Y1)
Fe2+(Y2)
Fe2+(Y3)
Fe3+
Fit SUM

Figure 4a

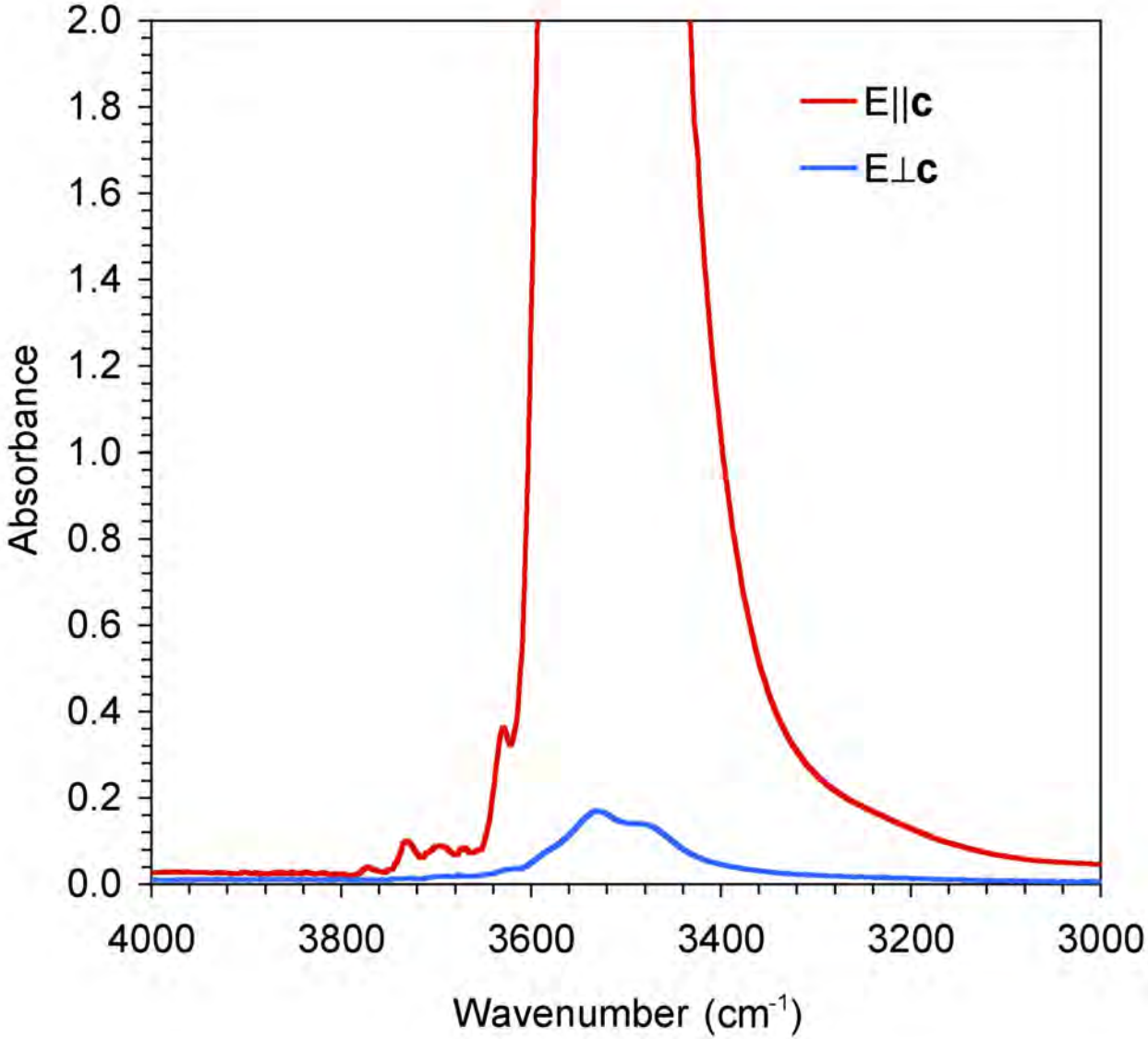
2.0
1.8
1.6
1.4
1.2
1.0
0.8
0.6
0.4
0.2
0.0
Absorbance
E||c
E⊥c
4000
3800
3600
3400
3200
3000
Wavenumber (cm-1)

Figure 4b

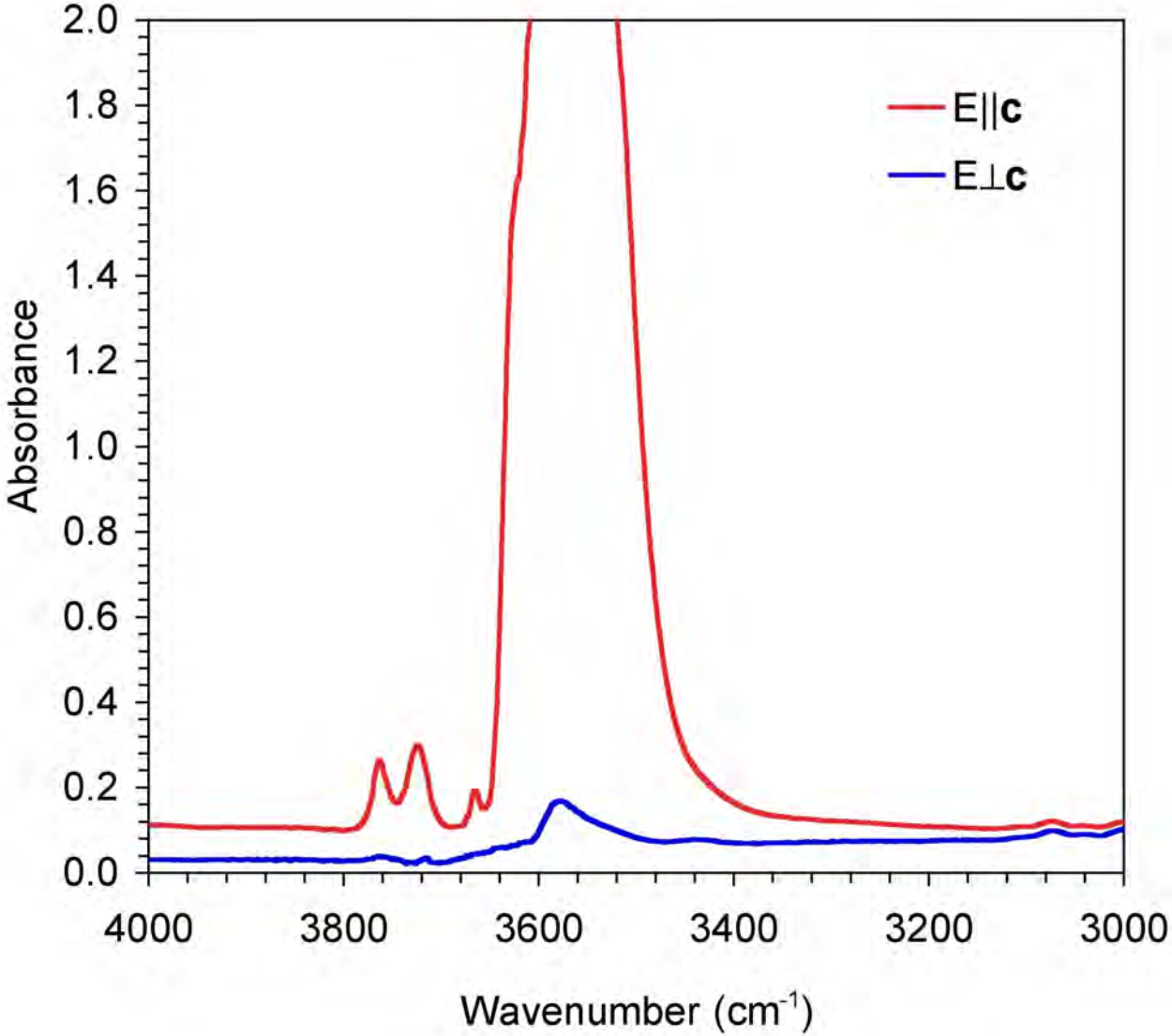
2.0
1.8
1.6
1.4
1.2
1.0
0.8
0.6
0.4
0.2
0.0
Absorbance
E||c
E⊥c
4000
3800
3600
3400
3200
3000
Wavenumber (cm-1)

Figure 5a

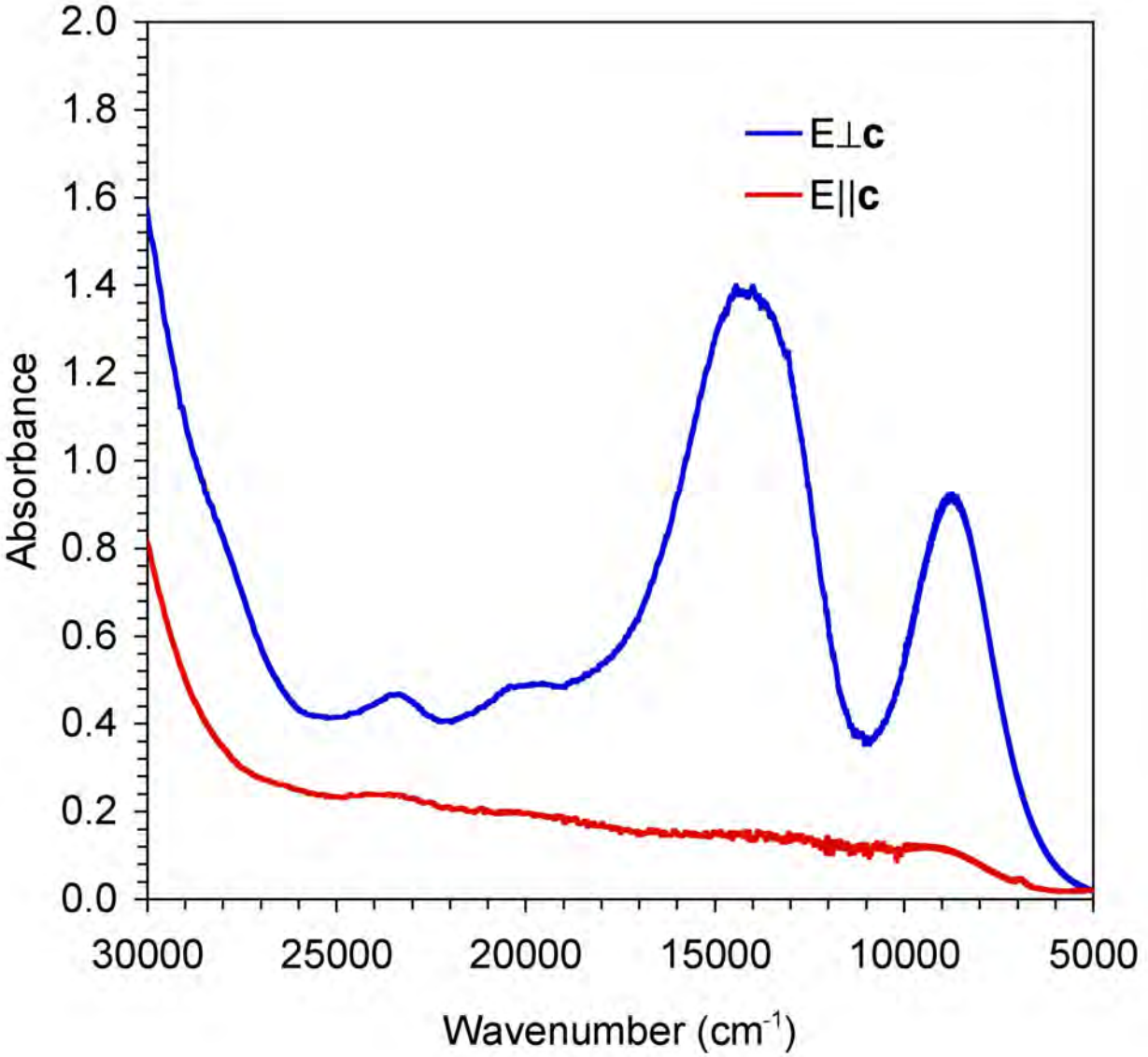
2.0
1.8
1.6
1.4
1.2
1.0
0.8
0.6
0.4
0.2
0.0
Absorbance
E⊥c
E||c
30000
25000
20000
15000
10000
5000
Wavenumber (cm-1)

Figure 5b

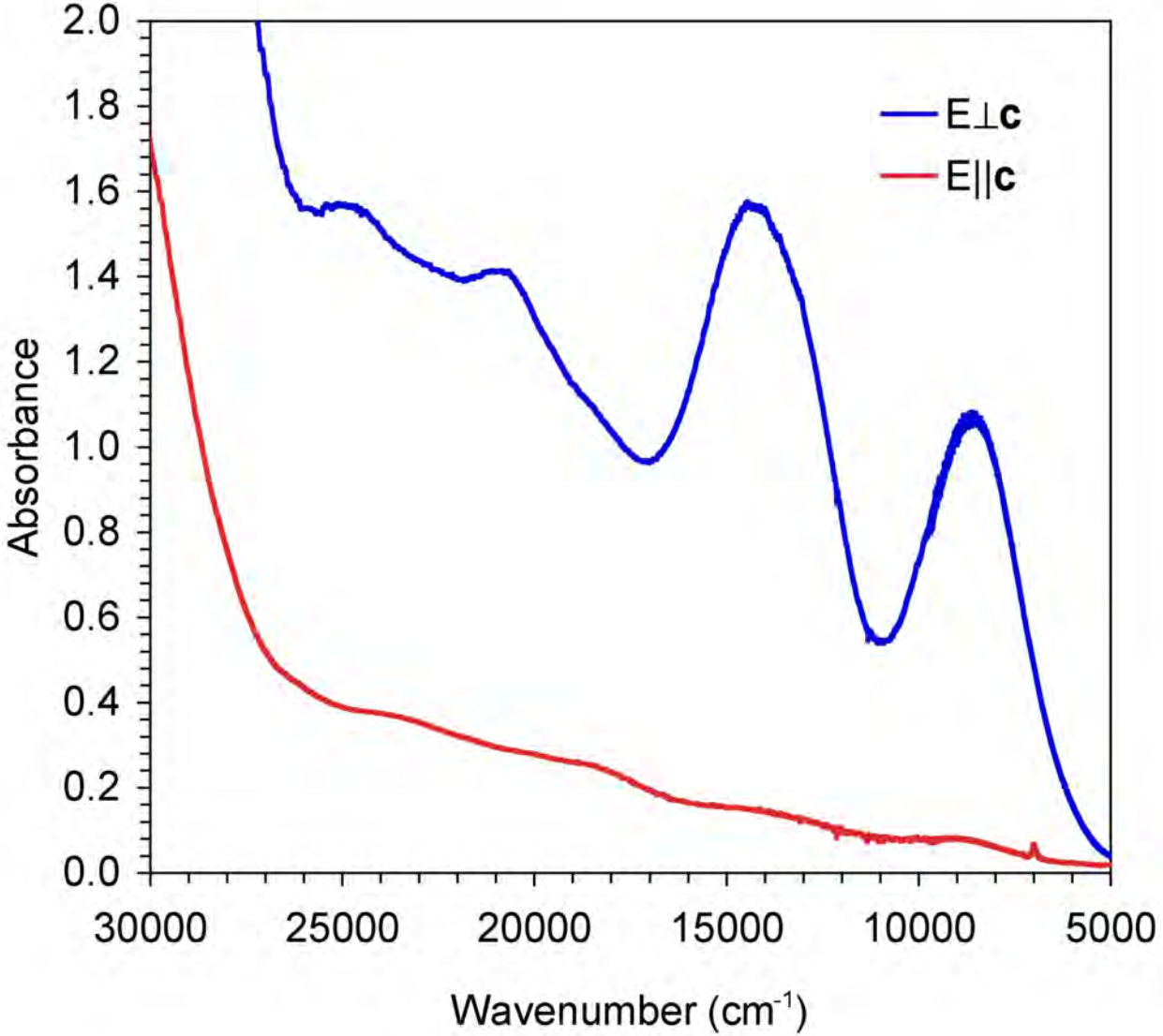
2.0
1.8
1.6
1.4
1.2
1.0
0.8
0.6
0.4
0.2
0.0
Absorbance
E⊥c
E||c
30000
25000
20000
15000
10000
5000
Wavenumber (cm-1)

Figure 6

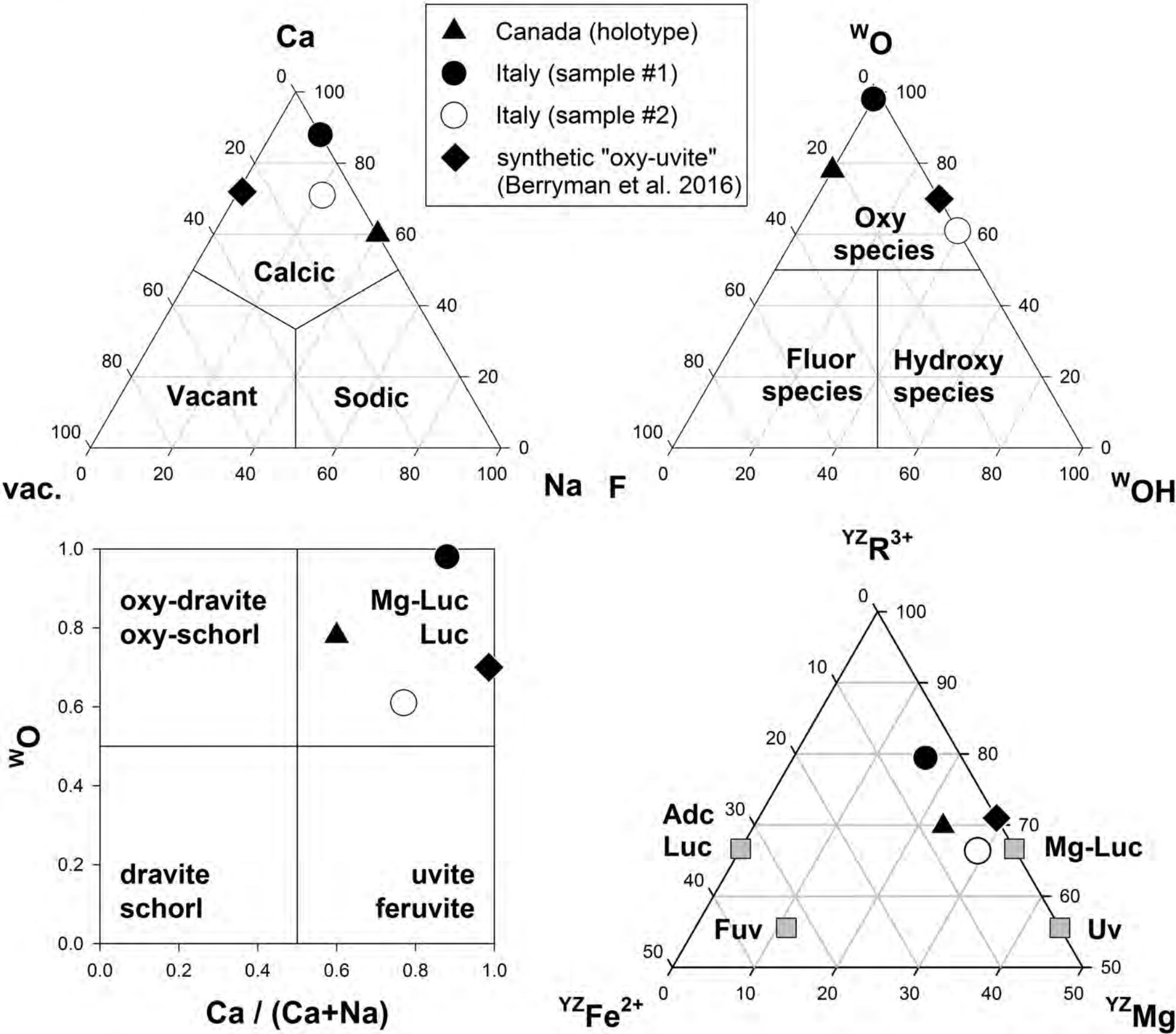
Canada (holotype)
Italy (sample #1)
Italy (sample #2)
synthetic "oxy-uvite" (Berryman et al. 2016)
Ca
vac.
Na
Calcic
Vacant
Sodic
^{W}O
F
^{W}OH
Oxy species
Fluor species
Hydroxy species
oxy-dravite
oxy-schorl
Mg-Luc
Luc
dravite
schorl
uvite
feruvite
^{W}O
Ca / (Ca+Na)
$^{YZ}R^{3+}$
Adc
Luc
Mg-Luc
Fuv
Uv
$^{YZ}Fe^{2+}$
^{YZ}Mg